mmol, 5 equiv) was added. After 30 min, the reaction was quenched with 10% NH_4Cl (0.5 mL) and allowed to warm to room temperature. The reaction was diluted in ether (20 mL), washed with 10% NH_4Cl (2 × 10 mL) and saturated NaCl (10 mL), dried over $MgSO_4$, filtered, and evaporated. Purification by flash chromatography on silica gel (pentane/ethyl acetate 60:1) gave **9** (55.4, 0.230 mmol) in 70% yield as a colorless liquid: IR (film) 2530 (s), 1715 (s), 1645 (m), 1630 (m), 1435 (m), 1420 (m), 1320 (s), 1285 (s), 1230 (s), 1190 (s), 1140 (s), 1100 (s) cm^{-1}; ^1H NMR (50.3 MHz, $CDCl_3$) 6.14 (d, J = 7.6 Hz, 1 H), 6.04 (d, J = 8.0 Hz, 1 H), 5.62 (dd, J = 8.2, 1.0 Hz, 1 H), 4.84 (dd, J = 9.3, 7.6 Hz, 1 H), 3.70 (s, 3 H), 2.17 (dd, J = 9.4, 1.0 Hz, 1 H), 1.47 (s, 3 H), −0.04 (s, 9 H); ^{13}C NMR (50.3 MHz, $CDCl_3$) 176.4, 140.4, 139.0, 110.0, 106.0, 52.0, 48.0, 39.2, 31.2, −1.57; mass spectrum, m/e 240.1179 (M^+ calcd for $C_{12}H_{20}O_3Si$ 240.1182), 225, 181, 165, 135, 121, 108, 73 (base).

Methyl *cis*-5-(Trimethylsilyl)-4,5-dihydrooxepin-4-carboxylate-4-*d* (10). **10** was prepared under similar conditions to those described for **9** with the substitution of methanol-*d* for methyl iodide; ^1H NMR (200 MHz, $CDCl_3$) 6.16 (d, J = 7.6 Hz, 1 H), 6.15 (d, J = 7.6 Hz, 1 H), 5.40 (d, J = 7.4 Hz, 1 H), 4.90 (t, J = 8.4 Hz, 1 H), 3.70 (s, 3 H), 2.41 (d, J = 8.8 Hz, 1 H), −0.06 (s, 9 H); ^{13}C NMR (50.3 MHz, $CDCl_3$) 173.1, 141.9, 139.9, 108.5, 105.2, 51.9, 43.8, (middle line of triplet), 33.1, −1.44.

Methyl 5-(Trimethylsilyl)-2,5-dihydrooxepin-4-carboxylate (11). IR (film) 2950 (m), 1715 (s), 1645 (m), 1430 (m), 1245 (s), 1125 (s), 1040 (m), 1020 (m) cm^{-1}; ^1H NMR (200 MHz, $CDCl_3$) 6.92 (t, J = 5.6 Hz, 1 H), 6.35 (dd, J = 7.1, 0.9 Hz, 1 H), 4.68 (m, 1 H), 4.66 (t, J = 7.4 Hz, 1 H), 4.31 (dd, J = 15.3, 5.6 Hz, 1 H), 3.74 (s, 3 H), 3.19 (br d, J = 7.4 Hz, 1 H), 0.075 (s, 9 H); ^{13}C NMR (50.3 MHz, $CDCl_3$) 167.8, 145.8. 137.4, 134.4, 108.6, 66.6, 52.1, 32.1, −1.98; mass spectrum, m/e 226.1024 (M^+ calcd for $C_{11}H_{18}O_3Si$ 226.1025), 225, 211, 195, 167, 151, 122, 73 (base).

Acknowledgment. We thank the Robert A. Welch Foundation and the National Institutes of Health (GM40033-01) for their generous support of this research. Exact mass spectral data were obtained from either the Michigan State University Mass Spectroscopy Facility (Dr. Douglas Gage), which is supported, in part, by a grant (DRR-00480) from the Biotechnology Research Branch, Division of Research Resources, National Institutes of Health, or the Department of Chemistry at The University of Texas at Austin (Dr. Mehdi Moini). We also thank Dr. David Colclough, Ms. Mahnaz Saffariannour, and Dr. Bela Derecskie for help in obtaining combustion analysis data. Purchase of the C,H,N analyzer through a grant from the Defense Advanced Research Projects Agency monitored by the Office of Naval Research is gratefully acknowledged.

Coordination Compounds of Polyoxovanadates with a Hexametalate Core. Chemical and Structural Characterization of $[V^V_6O_{13}\{(OCH_2)_3CR\}_2]^{2-}$, $[V^V_6O_{11}(OH)_2\{(OCH_2)_3CR\}_2]$, $[V^{IV}_4V^V_2O_9(OH)_4\{(OCH_2)_3CR\}_2]^{2-}$, and $[V^{IV}_6O_7(OH)_6\{(OCH_2)_3CR\}_2]^{2-}$

Qin Chen,[†] David P. Goshorn,[‡] Charles P. Scholes,[§] Xiao-ling Tan,[§] and Jon Zubieta*,[†]

Contribution from the Department of Chemistry, Syracuse University, Syracuse, New York 13244, Department of Chemistry, State University of New York at Albany, Albany, New York 12222, and Exxon Research and Engineering Co., Annandale, New Jersey 08801.
Received November 26, 1991

Abstract: Reactions of the tris(hydroxymethyl)methane-derived ligands, $(HOCH_2)_3Cr$, R = NO_2, CH_2OH, and CH_3, with $[(C_4H_9)_4N]_3[H_3V_{10}O_{28}]$ in CH_3CN yield the polyoxovanadate coordination complexes $[(C_4H_9)_4N]_2[V_6O_{13}\{(OCH_2)_3Cr\}_2]$ (R = NO_2, **1**; CH_2OH, **2**; CH_3, **3**). Complexes of this general class are electrochemically active, displaying a reversible one-electron reduction in the range −0.67 to −1.20 V, relative to the ferrocene/ferrocenium couple. The reduced species $[V^{IV}V^V_5O_{13}\{(OCH_2)_3CNO_2\}_2]^{3-}$ exhibits an eight-line EPR spectrum at 4.2 K, approximately centered at g = 1.95. Broadening of EPR spectral features as the temperature is raised from 4.2 to 83 K is evidence for increased motion of the unpaired electron consistent with thermally induced electron transfer between V^{IV} and V^V states. In contrast, chemical reductions of $[(C_4H_9)_4N]_2[V_6O_{13}\{(OCH_2)_3CCH_3\}_2]$ with organohydrazines yield the reduced, hydroxy-bridged species $[(C_4H_9)_4N]_2[V^{IV}_4V^V_2O_9(OH)_4\{(OCH_2)_3CCH_3\}_2]$ (**6**) and $[(C_4H_9)_4N]_2[V^{IV}_6O_7(OH)_6\{(OCH_2)_3CCH_3\}_2]\cdot 2CH_2Cl_2\cdot 0.5C_6H_5NNC_6H_5$ (**7**). The protonation sites have been established by X-ray crystallography. Protonation and reduction can be decoupled such that reaction of **3** with $HBF_4\cdot O(C_2H_5)_2$ yields the diprotonated species $[V_6O_{11}(OH)_2\{CH_3C(CH_2O)_3\}_2]$ (**5**) wherein the site of protonation has been established by X-ray crystallography as two of the bridging oxo groups. Crystal data are as follows. **1**: triclinic $P\bar{1}$; a = 11.470 (2) Å, b = 12.149 (2) Å, c = 12.433 (2) Å, α = 63.24 (1)°, β = 63.45 (1)°, γ = 79.31 (1)°, V = 1383.5 (5) Å^3, Z = 1, D_{calcd} = 1.55 g cm^{-3}; structure solution and refinement (in all cases: Mo Kα, λ = 0.710 73 Å) converged at R = 0.049. **2**·DMF: monoclinic $P2_1/c$, a = 12.003 (2) Å, b = 16.900 (3) Å, c = 16.769 (3) Å, β = 106.95 (1)°, V = 3253.8 (11) Å^3, Z = 2, D_{calcd} = 1.37 g cm^{-3}; R = 0.054. **3**: triclinic $P\bar{1}$, a = 11.460 (2) Å, b = 12.237 (2) Å, c = 12.331 (2) Å, α = 62.88 (1)°, β = 63.50 (1)°, γ = 77.52 (1)°, V = 1377.4 (5) Å^3, Z = 1, D_{calcd} = 1.49 g cm^{-3}; R = 0.055. **5**·2DMF·$(C_2H_5)_2O$: triclinic $P\bar{1}$, a = 10.362 (3) Å, b = 10.513 (3) Å, c = 10.366 (2) Å, α = 116.33 (1)°, β = 93.56 (1)°, γ = 62.40 (1)°, V = 882.2 (7) Å^3, Z = 1, D_{calcd} = 1.83 g cm^{-3}; R = 0.043. **6**: triclinic $P\bar{1}$, a = 11.534 (2) Å, b = 12.161 (3) Å, c = 12.483 (4) Å, α = 62.86 (2)°, β = 63.15 (2)°, γ = 78.87 (2)°, V = 1389.7 (7) Å^3, Z = 1, D_{calcd} = 1.48 g cm^{-3}; R = 0.043. **7**: triclinic $P\bar{1}$, a = 13.613 (3) Å, b = 16.090 (4) Å, c = 16.077 (4) Å, α = 86.36 (1)°, β = 80.71 (2)°, γ = 80.46 (1)°, V = 3424.1 (12) Å^3, Z = 2, D_{calcd} = 1.45 g cm^{-3}; R = 0.042.

Polyoxometalates are a class of soluble molecular oxides which incorporate structural characteristics of the more complex solid oxide surfaces used in a variety of heterogeneous catalysis processes.[1-3] This structural analogy between polyoxometalates and

[†] Syracuse University.
[‡] Exxon Research and Engineering Co.
[§] State University of New York at Albany.

(1) Day, V. W.; Klemperer, W. G. *Science (Washington, D.C.)* **1985**, *228*, 533.

0002-7863/92/1514-4667$03.00/0

metal oxide surfaces has been responsible in large measure for the dramatic expansion of the coordination chemistry of polyoxomolybdates with a variety of oxygen,[4] nitrogen,[5] and even sulfur donors.[6] In contrast, the coordination chemistry of polyoxovanadate derivatives remains relatively unexplored. However, the recent isolation and characterization of several polyvanadate tetra-*n*-butylammonium salts soluble in aprotic polar solvents, such as $[(n\text{-}C_4H_9)_4N]_3[H_3V_{10}O_{28}]$,[7] $[(n\text{-}C_4H_9)_4N]_4[V_{12}O_{32}(CH_3CN)]$,[8] and $[(n\text{-}C_4H_9)_4N]_3[V_5O_{14}]$,[9] provide a starting point for the synthesis of covalent polyoxovanadate species. Exploiting the reactivity of $[H_3V_{10}O_{28}]^{3-}$ toward hydroxylic oxygen donors in methylene chloride and acetonitrile, we have recently isolated and described the polyoxovanadate coordination complexes $[(n\text{-}C_4H_9)_4N]_2[V_8O_8(OCH_3)_{16}(C_2O_4)]$[10] and $[(n\text{-}C_4H_9)_4N]_2[V_6O_{13}\{(OCH_2)_3CNO_2\}_2]$.[11] Other polyoxovanadate–ligand aggregates have also been synthesized by employing alternate synthetic routes,[12] suggesting that polyoxovanadates possess a rich coordination chemistry with unique structural types not encountered for the polyoxomolybdates.

We report here the syntheses and characterization of polyhydroxylic hexavanadate derivatives $[(n\text{-}C_4H_9)_4N]_2[V_6O_{13}\{(OCH_2)_3CR\}_2]$ and of the products of coupled reduction and protonation $[(n\text{-}C_4H_9)_4N]_2[V_6O_9(OH)_4\{(OCH_2)_3CCH_3\}_2]$ and $[(n\text{-}C_4H_9)_4N]_2[V_6O_7(OH)_6\{(OCH_2)_3CCH_3\}_2]$ and of protonation decoupled from reduction $[V_6O_{11}(OH)_2\{(OCH_2)_3CCH_3\}_2]$. The hexametalate unit $[M_6O_{19}]^{n-}$ not only is a common structural type for early transition metal polyoxoanion derivatives but, furthermore, serves as a framework for the incorporation of inorganic, organometallic, or organic moieties bound to one or more[13] of the approximately coplanar, closest-packed oxygens which constitute the faces of the hexametalate anion.[1,7] Although this hexametalate core has been described only recently in polyvanadate chemistry, the structural variations observed in comparing the structures of $[V_6O_{13}(OCH_2)_3Cr\}_2]^{2-}$[11] and $[(C_5H_5)Rh]_4[V_6O_{19}]$[14] reveal that significant distortions from the more or less regular $[M_6O_{19}]^{n-}$ "superoctahedral" core may be tolerated, via expansion either of the triangular faces of closest-packed oxygens or of the spacing between approximately planar layers of negatively charged, close-packed oxygen atoms as shown below.

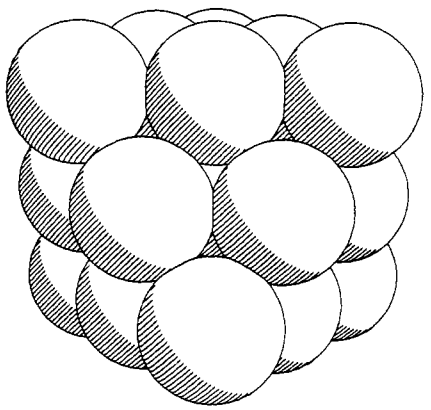

(2) Pope, M. T. *Heteropoly and Isopoly Oxometalates*; Springer-Verlag: New York, 1983.

(3) Campbell, I. M. *Catalysis at Surfaces*; Chapman and Hall: New York, 1988.

(4) (a) $[Mo_8O_{24}(OCH_3)_4]^{4-}$: McCarron, E. M., III; Harlow, R. L. *J. Am. Chem. Soc.* **1983**, *105*, 6179. (b) $[(HCO)_2Mo_8O_{28}]^{6-}$: Adams, R. D.; Klemperer, W. G.; Liu, R.-S. *J. Chem. Soc., Chem. Commun.* **1979**, *256*. (c) $[CH_2Mo_4O_{15}H]^{3-}$: Day, V. W.; Frederick, M. F.; Klemperer, W. G.; Liu, R.-S. *J. Am. Chem. Soc.* **1979**, *101*, 491. (d) $[Mo_4O_8(OC_2H_5)_2\{(OCH_2)_2CCH_3\}_2]$: Wilson, A. J.; Robinson, W. T.; Wilkinson, C. J. *Acta Crystallogr.* **1983**, *C39*, 54. (e) $[Mo_4O_8(OCH_3)_2]HB(py)_3]_2(HOCH_3)_2]$, $HB(py)_3^-$ = hydrotripyrazolylborate: Linclon, S.; Koch, S. A. *Inorg. Chem.* **1986**, *25*, 1594. (f) $[Mo_4O_6Cl_2(O_2CCH_3)_6]$: Kamenar, B.; Korpar-Colig, B.; Penanic, M. *J. Chem. Soc., Dalton Trans.* **1981**, 311. (g) $[Mo_4O_{11}(citrate)_2]^{4-}$: Nassimbeni, L. R.; Niven, M. L.; Crwywagen, J. I.; Heyns, B. B. *J. Crystallogr. Spectrosc. Res.* **1982**, *17*, 373. Alcock, N. W.; Dudek, M.; Grybos, R.; Hodorowicz, E.; Kanas, A.; Samotus, A. *J. Chem. Soc., Dalton Trans.* **1990**, 707. (h) $[Mo_4O_6Cl_2(O_2C_6H_4CH_3)_6]$: Chunting, S.; Chunxiao, G.; Yan, J.; Tiejin, L.; Ling, Y.; Yuguo, F. *Eur. J. Solid State Inorg. Chem.* **1989**, *26*, 231. (i) $[Mg_2Mo_8O_{22}(OCH_3)_6(HOCH_3)_4]^{2-}$: Antipin, M. Y.; Lidenko, L. P.; Kachapina, L. M.; Shilov, A. G.; Shilova, A. K.; Struchkov, Y. T. *J. Chem. Soc., Chem. Commun.* **1989**, 1467. (j) $[Mo_4O_{11}(malate)_2]^{4-}$: Porai-Koshits, M. A.; Aslanov, L. A.; Ivanova, A. G.; Polynova, T. N. *J. Struct. Chem. (Engl. Transl.)* **1968**, *9*, 401. Knobler, C. B.; Wilson, A. J.; Hider, R. N.; Jensen, I. W.; Penfold, B. R.; Robinson, W. T.; Wilkins, C. J. *J. Chem. Soc., Dalton Trans.* **1983**, 1299. (k) $[Mo_8O_{22}(OH)_4(OC_6H_5CH{=}NPr)_2]^{2-}$ and $[Mo_8O_{24}(OH)_2(Omet)_2]^{4-}$, Omet = methionate: Kamenar, B.; Korpar-Colig, B.; Penanic, M.; Cindric, M. *J. Chem. Soc., Dalton Trans.* **1990**, 1125. (l) $[Mo_4O_{10}(OCH_3)_6]^{2-}$: Liu, S.; Shaikh, S. N.; Zubieta, J. *Inorg. Chem.* **1987**, *26*, 4303. (m) $[Mo_8O_{22}(OH)_2(OCH_3)_2]^{4-}$: Liu, S.; Zubieta, J. *Polyhedron* **1989**, *8*, 537. (n) $[Mo_4O_8(OCH_3)_2(C_4O_4)_2(C_4O_4H)_2]$: Chen, Q.; Liu, S.; Zubieta, J. *Inorg. Chim. Acta* **1989**, *164*, 115. (o) $[Mo_{12}O_{36}(C_4O_4H)_4]^{4-}$: Chen, Q.; Liu, S.; Zubieta, J. *Angew Chem., Int. Ed. Engl.* **1990**, *29*, 70. (p) $[Mo_3O_8(OCH_3)(C_4O_4)_2]^{3-}$: Chen, Q.; Ma, L.; Liu, S.; Zubieta, J. *J. Am. Chem. Soc.* **1989**, *111*, 5944. (q) $[Mo_8O_{16}(OCH_3)_8(C_2O_4)]^{2-}$: Chen, Q.; Liu, S.; Zubieta, J. *Angew Chem., Int. Ed. Engl.* **1988**, *27*, 1724. (r) $[RMo_4O_{15}X]^{3-}$, R = C_9H_4O, X = OCH_3; R = $C_{14}H_{10}$, X = $C_7H_5O_2$: Chen, Q.; Liu, S.; Zhu, H.; Zubieta, J. *Polyhedron* **1989**, *8*, 2915. R = $C_{14}H_8$, X = OH: Liu, S.; Shaikh, S. N.; Zubieta, J. *Inorg. Chem.* **1988**, *27*, 3066.

(5) (a) $[Mo_8O_{26}(NC_5H_5)_2]^{4-}$: McCarron, E. M., III; Whitney, J. F.; Chase, D. B. *Inorg. Chem.* **1984**, *23*, 3275. (b) $[Mo_4O_{12}(C_{12}H_{30}N_4S_2)_2]$: Hursthouse, M. B.; Short, R. L.; Piggott, B.; Trecher, A.; Wong, S. F. *Polyhedron* **1986**, *5*, 2121. (c) $[Mo_4O_{12}\{CH_3C(NH)NO\}_2]^{2-}$: Chilou, V.; Gouzerh, P.; Jeannin, Y.; Robert, F. *J. Chem. Soc., Chem. Commun.* **1982**, 1469. (d) $[Mo_4O_{11}\{tolC(NH_2)NHO\}_2\{tolC(NH)NHO\}\{tolC(CNH)NO\}]^{-}$: Chilou, V.; Gouzerh, P.; Jeannin, Y.; Robert, F. *J. Chem. Soc., Chem. Commun.* **1987**, 1469. (e) $[NaMo_5O_{13}(OCH_3)_4(NO)]^{2-}$: Gouzerh, P.; Jeannin, Y.; Proust, A.; Robert, F. *Angew Chem., Int. Ed. Engl.* **1989**, *28*, 1363. (f) $[Mo_4O_{11}(dhphH_2)]^{2-}$, $dhphH_2$ = dihydrazido(2−)phthalazine: Attanasio, D.; Fares, V.; Imperatori, P. *J. Chem. Soc., Chem. Commun.* **1986**, 1476. (g) $[Mo_8O_{26}(NCS)_2]^{6-}$: Kamenar, B.; Penavic, M.; Markovic, B. *Acta Crystallogr., Sect. C.* **1988**, *44*, 3275. (h) $[Mo_4O_8(OCH_3)_2(NNR)_4]^{2-}$: Hsieh, T.-C.; Zubieta, J. *Inorg. Chem.* **1985**, *24*, 1287. Hsieh, T.-C.; Zubieta, J. *Polyhedron* **1985**, *5*, 309. (i) $[Mo_8O_{20}(NNPh)_6]^{4-}$: Hsieh, T.-C.; Zubieta, J. *J. Chem. Soc., Chem. Commun.* **1985**, 1749. (j) $[Mo_4O_{10}(OMe_2)_2(NNPh)_2]^{2-}$: Hsieh, T.-C.; Shaikh, S. N.; Zubieta, J. *Inorg. Chem.* **1987**, *26*, 4079. (k) $[Mo_4O_{12}(C_8H_6N_4)]^{2-}$: Shaikh, S. N.; Zubieta, J. *Inorg. Chem.* **1988**, *27*, 1896. (l) $[Mo_6O_{18}(NNPh)]^{3-}$: Hsieh, T.-C.; Zubieta, J. *Polyhedron* **1986**, *5*, 1658. (m) $[Mo_6O_{18}(NNMePh)]^{2-}$: Kang, H.; Zubieta, J. *J. Chem. Soc., Chem. Commun.* **1988**, 1192. (n) $[Mo_4O_{10}(OCH_3)_2(NNMePh)_2]^{2-}$: Shaikh, S. N.; Zubieta, J. *Inorg. Chem.* **1986**, *25*, 4613. (o) $[Mo_4O_6(OCH_3)_2(C_{10}H_6O_2)_2(NNPh)_4]^{2-}$: Kang, H.; Shaikh, S. N.; Nicholson, T.; Zubieta, J. *Inorg. Chem.* **1989**, *28*, 920.

(6) $[Mo_{10}O_{28}(SCH_2CH_2O)_2(HOCH_3)_2]^{4-}$: Liu, S.; Sun, X.; Zubieta, J. *J. Am. Chem. Soc.* **1988**, *110*, 3324.

(7) Day, V. W.; Klemperer, W. G.; Maltbie, D. J. *J. Am. Chem. Soc.* **1987**, *109*, 2991.

(8) Day, V. W.; Klemperer, W. G.; Yaghi, O. M. *J. Am. Chem. Soc.* **1989**, *111*, 5959.

(9) Day, V. W.; Klemperer, W. G.; Yaghi, O. M. *J. Am. Chem. Soc.* **1989**, *111*, 4519.

(10) Chen, Q.; Liu, S.; Zubieta, J. *Inorg. Chem.* **1989**, *28*, 4434.

(11) Chen, Q.; Zubieta, J. *Inorg. Chem.* **1990**, *29*, 1456.

(12) (a) $[VO(salicylhydroximate)(CH_3OH)]_3$: Pecoraro, V. L. *Inorg. Chim. Acta* **1989**, *155*, 171. (b) $[V_6O_{10}(O_2CPh)_6]$: Rehder, D.; Priebsch, W.; von Oegnhausen, M. *Angew. Chem., Int. Ed. Engl.* **1989**, *28*, 1221. (c) $[V_5O_9Cl(tca)_4]^{2-}$ and $[V_4O_8(NO_3)(tca)_4]^{2-}$, tca = thiophene-2-carboxylate: Heinrich, D. D.; Folting, K.; Streib, W. E.; Huffman, J. C.; Christou, G. *J. Chem. Soc., Chem. Commun.* **1989**, 1411. (d) $[V_4O_8(C_2O_4)_4(H_2O)_2]^{4-}$: Reiskamp, H.; Gietz, P.; Mattes, R. *Chem. Ber.* **1976**, *109*, 2090. (e) $[V_9O_{16}(butanediaminetetraacetic\ acid)_4]^{7-}$: Launay, J.-P.; Jeannin, Y.; Daoudi, M. *Inorg. Chem.* **1985**, *24*, 1052. (f) $[V_{15}O_{36}(CO_3)]^{7-}$: Müller, A.; Penk, M.; Rohlfing, R.; Krickemeyer, E.; Döring, J. *Angew. Chem., Int. Ed. Engl.* **1990**, *29*, 926. (g) $[V_{12}As_8O_{40}(HCO_2)]^{n-}$: Müller, A.; Döring, J.; Bögge, H. *J. Chem. Soc., Chem. Commun.* **1991**, 273.

(13) (a) $[HNb_6O_{19}]^{7-}$: Lindquist, I. *Ark. Kemi.* **1953**, *5*, 247. (b) $[HV_2W_4O_{19}]^{3-}$: Flynn, C. M., Jr.; Pope, M. T. *Inorg. Chem.* **1971**, *10*, 4091. (c) $[(C_5H_5)_3Ac(MW_5O_{19})_2]^{5-}$, Ac = Th, U and M = Nb, Ta: Day, V. W.; Klemperer, W. G.; Maltbie, D. J. *Organometallics* **1985**, *4*, 104. (d) $\{[(C_5H_5)_2U]_2[TiW_5O_{19}]_2\}^{4-}$: Day, V. W.; Earley, C. W.; Klemperer, W. G.; Maltbie, D. J. *J. Am. Chem. Soc.* **1985**, *107*, 8261. (e) $[M(Nb_6O_{19})_2]^{12-}$, M = Mn, Ni: Flynn, C. M., Jr.; Stucky, G. D. *Inorg. Chem.* **1969**, *8*, 335. Flynn, C. M., Jr.; Stucky, G. D. *Inorg. Chem.* **1969**, *8*, 332. Iale, B. W.; Pope, M. T. *J. Chem. Soc., Chem. Commun.* **1967**, *792*. (f) $[(H_2O)(en)M(Nb_6O_{19})]^{5-}$, M = Cr, Co: Flynn, C. M., Jr.; Stucky, G. D. *Inorg. Chem.* **1969**, *8*, 178. (g) $[(CO)_3M(Nb_2W_4O_{19})]^{3-}$, M = Mn, Re: Besecker, C. J.; Day, V. W.; Klemperer, W. G.; Thompson, M. R. *Inorg. Chem.* **1985**, *24*, 44. Besecker, C. J.; Klemperer, W. G. *J. Am. Chem. Soc.* **1980**, *102*, 7598. (h) $\{[(CH_3)_5C_5Rh][Nb_2W_4O_{19}]\}^{2-}$: Besecker, C. J.; Day, V. W.; Klemperer, W. G.; Thompson, M. R. *J. Am. Chem. Soc.* **1984**, *106*, 4125. (i) $\{[(C_7H_8)Rh]_5[Nb_6W_4O_{19}]_2\}^{3-}$: Besecker, C. J.; Klemperer, W. G.; Day, V. W. *J. Am. Chem. Soc.* **1982**, *104*, 6158. (j) $[Nb_2W_4O_{19}R]^{3-}$, R = CH_3, $Si(CH_3)_2[C(CH_3)_3]$: Day, V. W.; Klemperer, W. G.; Schwartz, C. *J. Am. Chem. Soc.* **1987**, *109*, 6030. (k) $[(C_5Me_5)_2(W_6O_{19})]$: Harper, J. R.; Rheingold, A. L. *J. Am. Chem. Soc.* **1990**, *112*, 4037.

(14) (a) Hayaski, Y.; Oxawa, Y.; Isobe, K. *Chem. Lett.* **1989**, 425. (b) Chae, H. K.; Klemperer, W. G. *Inorg. Chem.* **1989**, *28*, 1423.

Although reduction of the hexametalate unit may be expected to result in expansion of the core,[15] the metrical parameters affected may be localized to interplanar separations or individual bond lengths or delocalized throughout the cluster. Similarly, protonation may occur at terminal or doubly bridging oxygen sites with some concomitant bond lengthening and cluster expansion.[16] The protonation behavior of other polyvanadates and vanadotungstates strongly suggested that the doubly bridging oxygens are considerably more basic than the terminal oxo groups.[7,13b,17] The structural investigations of the complexes of this study confirm the bridging oxygens as the sites of protonation and demonstrate the consequences of sequential reduction and protonation on the cluster dimensions of the "$[V_6O_{19}]^{8n}$" core.

Experimental Section

All chemicals were obtained from either Aldrich, Alfa, or Eastman. The precursor isopolyoxovanadate $[H_3V_{10}O_{28}]^{3-}$ was prepared by the literature method.[7] All manipulations were carried out under purified N_2 by using standard Schlenk techniques. Methanol and methylene chloride were dried over magnesium methoxide and CaH_2, respectively. Anhydrous ether was passed through activated alumina prior to use. Elemental analyses were performed by Desert Analytics, Tucson, AZ.

The ligands $RC(CH_2OH)_3$ (R = CH_3, CH_2CH_3, CH_2OH, NO_2, and NH_2) were purchased from Aldrich Chemical Co. The derivative $(CH_3)_2NC(CH_2OH)_3$ was prepared by methylation of 1,1,1-tris(hydroxymethyl)aminomethane. The ligand $C_6H_5CH_2C(CH_2OH)_3$ was prepared from the reaction of α-bromotoluene with $NaC(CO_2C_2H_5)_3$ in DMF,[18] followed by reduction with $LiAlH_4$.[19]

The following instruments were used in this work: IR, Perkin-Elmer 283B infrared spectrophotometer; UV–visible, Varian DMSO 90 UV–visible spectrophotometer; X-ray crystallography, Siemens R3m/V diffractometer and Rigaku AFC5S diffractometer; electrochemistry, BAS100 electroanalytical system; NMR, Varian XL-300 spectrometer.

Cyclic voltammetric studies and controlled potential electrolyses were carried out in acetonitrile or dimethylformamide solution 1.0×10^{-3} M in complex and 0.1 M in $(n\text{-}C_4H_9)_4NPF_6$ as supporting electrolyte. Platinum bead and platinum mesh working electrodes were used in the cyclic voltammetry and controlled potential electrolysis, respectively. All potentials are referenced to the ferrocene/ferrocenium couple.

Preparation of $[(n\text{-}C_4H_9)_4N]_2[V_6O_{13}\{(OCH_2)_3CNO_2\}_2]$ (1). Tris(hydroxymethyl)nitromethane (0.45 g, 3.0 mmol) was added to a solution of $[(n\text{-}C_4H_9)_4N]_3[H_3V_{10}O_{28}]$ (1.69 g, 1.0 mmol) in CH_3CN (50 mL) with stirring. The yellow-brown solution obtained upon refluxing for 24 h was cooled to room temperature and reduced in volume to 25 mL by rotary evaporation. Upon addition of 25 mL of diethyl ether, a reddish brown powder was obtained (1.25 g). Recrystallization from DMF/CH_3CN/diethyl ether (1:1:2 v/v/v) yielded red crystals in 45% yield. The crystalline product is indefinitely stable when exposed to the atmosphere, while solutions of the complex decompose over a period of days when exposed to the atmosphere at room temperature. Anal. Calcd for $C_{40}H_{84}N_4O_{23}V_6$: C, 37.1; H, 6.49; N, 4.33. Found: C, 37.2; H, 6.32; N, 4.26. IR (KBr pellet, cm^{-1}): 2959 (m), 1531 (m), 1335 (w), 1260 (s), 1083 (s), 1022 (m), 960 (m), 944 (s), 800 (s), 719 (m), 410 (m). UV/vis [DMF; λ_{max}, nm (ϵ, cm^{-1} M^{-1})]: 274 (7400), 384 (2500).

Preparations of $[(n\text{-}C_4H_9)_4N]_2[V_6O_{13}\{(OCH_2)_3CCH_2OH\}_2]$ (2), $[(n\text{-}C_4H_9)_4N]_2[V_6O_{13}\{(OCH_2)_3CCH_3\}_2]$ (3), $[(n\text{-}C_4H_9)_4N]_2[V_6O_{13}\{(OCH_2)_3CCH_2CH_3\}_2]$ (3a), $[(n\text{-}C_4H_9)_4N]_2[V_6O_{13}\{(OCH_2)_3CNMe_2\}_2]$ (4), and $[(n\text{-}C_4H_9)_4N]_2[V_6O_{13}\{(OCH_2)_3CCH_2C_6H_5\}_2]$ (4a). The complexes $[(n\text{-}C_4H_9)_4N]_2[V_6O_{13}\{(OCH_2)_3CCH_2O\}_2]$ (2), $[(n\text{-}C_4H_9)_4N]_2[V_6O_{13}\{(OCH_2)_3CCH_3\}_2]$ (3), $[(n\text{-}C_4H_9)_4N]_2[V_6O_{13}\{(OCH_2)_3CCH_2CH_3\}_2]$ (3a), $[(n\text{-}C_4H_9)_4N]_2[V_6O_{13}\{(OCH_3)_3CNMe_2\}_2]$ (4), and $[(n\text{-}C_4H_9)_4N]_2[V_6O_{13}\{(OCH_2)_3CCH_2C_6H_5\}_2]$ (4a) were prepared by similar synthetic procedures using the appropriate tris(hydroxymethyl)methane derivative.

Anal. Calcd for $C_{45}H_{97}N_3O_{22}V_6$ (2·DMF): C, 40.4; H, 7.26; N, 3.14. Found: C, 40.2; H, 7.19; N, 3.06. IR (KBr pellet, cm^{-1}): 3350 (m), 2959 (m), 2865 (m), 1660 (s), 1485 (m), 1392 (w), 1378 (w), 1255 (w), 1120 (m), 1078 (w), 1038 (m), 950 (vs), 810 (m), 796 (m), 715 (s), 658 (w), 585 (w), 420 (m). UV/vis [DMF; λ_{max}, nm (ϵ, cm^{-1} M^{-1})]: 275 (14000), 357 (6500).

Anal. Calcd for $C_{42}H_{90}N_2O_{19}V_6$ (3): C, 40.9; H, 7.31; N, 2.27. Found: C, 40.8; H, 7.35; N, 2.16. IR (KBr pellet, cm^{-1}): 2959 (m), 2865 (m), 1483 (m), 1460 (m), 1386 (w), 1250 (s), 1130 (m), 960 (s), 940 (vs), 816 (m), 792 (m), 710 (s), 610 (w), 570 (w), 410 (m). UV/vis [DMF; λ_{max}, nm (ϵ, cm^{-1} M^{-1})]: 275 (13000), 338 (6100).

Anal. Calcd for $C_{44}H_{94}N_2O_{19}V_6$ (3a): C, 41.9; H, 7.46; N, 2.22. Found: C, 41.7; H, 7.62; N, 2.18. IR (KBr pellet, cm^{-1}): 2960 (m), 2870 (m), 1475 (m), 1450 (m), 1370 (w), 1140 (m), 1250 (s), 955 (s), 815 (m), 792 (m), 750 (s), 710 (s), 410 (m). UV/vis [DMF; λ_{max}, nm (ϵ, cm^{-1} M^{-1})]: 270 (1200), 340 (5500).

Anal. Calcd for $C_{44}H_{96}N_4O_{19}V_6$ (4): C, 40.9; H, 7.44; N, 4.34. Found: C, 40.9; H, 7.32; N, 4.10. IR (KBr pellet, cm^{-1}): 2955 (m), 2865 (m), 1485 (m), 1420 (m), 1380 (w), 1250 (m), 1172 (m), 950 (vs), 820 (m), 790 (m), 720 (s), 630 (w), 582 (w), 415 (m). UV/vis [DMF; λ_{max}, nm (ϵ, cm^{-1} M^{-1})]: 275 (12000), 345 (6300).

Anal. Calcd for $C_{54}H_{98}N_2O_{19}V_6$ (4a): C, 46.8; H, 7.08; N, 2.02. Found: C, 46.7; H, 7.24; N, 2.22. IR (KBr pellet, cm^{-1}): 3110 (m), 2955 (m), 2865 (m), 1480 (m), 1445 (m), 1370 (m), 1745 (s), 1140 (m), 950 (s), 815 (m), 790 (m), 740 (s), 705 (s) 685 (s), 405 (m). UV/vis [DMF; λ_{max}, nm (ϵ, cm^{-1} M^{-1})]: 270 (12500), 345 (5700).

Preparation of $[V_6O_{11}(OH)_2\{(OCH_2)_3CCH_3\}_2]$ (5). $[(n\text{-}C_4H_9)_4N]_2[V_6O_{13}\{(OCH_2)_3CCH_3\}_2]$ (3) (0.61 g, 0.5 mmol) was placed in a rigorously dried, argon-purged Schlenk flask and dissolved in CH_2Cl_2 (25 mL). A solution of $HBF_4{\cdot}O(C_2H_5)_2$ (0.243 g) was added dropwise and the solution stirred for 2 h. The resultant red precipitate was collected and dissolved in a minimum of DMF. After careful layering of this solution with diethyl ether, the solution was allowed to stand at 4 °C for 5 days. The red crystals of needle habit of 5·2DMF·$(C_2H_5)_2O$ which deposited were collected, washed with ether, and dried under nitrogen. Yield: 35%. Anal. Calcd for $C_{20}H_{44}N_2O_{22}V_6$ (5·2DMF·$(C_2H_5)_2O$): C, 24.7; H, 4.54; N, 2.89. Found: C, 24.6; H, 4.59; N, 2.76. IR (KBr pellet, cm^{-1}): 2950 (w), 2880 (w), 1647 (s), 1432 (m), 1364 (m), 1130 (m), 1039 (s), 954 (s), 796 (m), 711 (m).

Preparation of $[V_6O_{11}(OSiMe_2Bu^t)_2\{(OCH_2)_3CCH_3\}_2]$ (5a). A solution of $(t\text{-}C_4H_9)(CH_3)_2SiOSO_2CF_3$ (Petrarch) (3 μL, 1.14 mmol) in 5 mL of CH_2Cl_2 was added to a solution of 3 (0.68 g, 0.57 mmol) in 10 mL of CH_2Cl_2. The solution was refluxed for 20 min and then allowed to cool to room temperature. Upon addition of 20 mL of diethyl ether, a bright red oil separated. The oil was taken up in 5 mL of acetonitrile which was carefully layered with 10 mL of diethyl ether. After 8 days at 4 °C, a fine red precipitate of $[V_6O_{11}(OSiMe_2Bu^t)_2\{(OCH_2)_3CCH_3\}_2]$ (5a) deposited on the walls of the container. The compound was collected by suction filtration and washed with diethyl ether. Yield: 32%. Anal. Calcd for $C_{22}H_{48}O_{19}Si_2V_6$: C, 27.0; H, 4.91. Found: C, 26.7; H, 4.72. IR (KBr pellet, cm^{-1}): 2964 (m), 2871 (m), 1483 (m), 1450 (m), 1370 (w), 1250 (m), 1125 (m), 952 (s), 790 (vs), 750 (m).

The complex $[V_6O_{11}(OSiMe_3)_2\{(OCH_2)_3CNO_2\}_2]$ (5b) was synthesized in a similar fashion from $(TBA)_2[V_6O_{13}\{(OCH_2)_3CNO_2\}_2]$ (1) and $ClSiMe_3$.

Preparation of $[(n\text{-}C_4H_9)_4N]_2[V_6O_{11}(OH)_2\{(OCH_2)_3CCH_3\}_2]$ (5c). Sodium acenaphthylenide was added to a solution of $[V_6O_{11}(OH)_2\{(OCH_2)_3CCH_3\}_2]$ (5) (0.750 g, 1 mmol) in acetonitrile (10 mL). Upon addition of $(n\text{-}C_4H_9)_4NCl$ in methanol (25 mL), a green-brown precipitated of 5c formed immediately. The solid was collected by filtration, washed with methanol, and dried in a stream of argon. Attempts to recrystallize 5c invariably gave mixtures of 3 and 6 as a result of disproportionation. Anal. Calcd for $C_{42}H_{92}N_2O_{19}V_6$: C, 40.8; H, 7.45; N, 2.27. Found: C, 40.6; H, 7.32; N, 2.00. IR (KBr pellet, cm^{-1}); 3450 (w), 2960 (m), 2870 (w), 1607 (w), 1490 (m), 1450 (m), 1378 (w), 1125 (m), 950 (vs), 750 (vs), 600 (w), 560 (m), 400 (m). UV/vis [CH_2Cl_2; λ_{max}, nm (ϵ, cm^{-1} M^{-1})]: 250 (16000), 310 (sh), 782 (410).

Preparation of $[(n\text{-}C_4H_9)_4N]_2[V_6O_9(OH)_4\{(OCH_2)_3CCH_3\}_2]$ (6). $[(n\text{-}C_4H_9)_4N]_2[V_6O_{13}\{(OCH_2)_3CCH_3\}_2]$ (3) (0.61 g, 0.5 mmol) was placed in a rigorously dried, argon-purged Schlenk flask. Upon dropwise addition with stirring of a solution of 1-methyl-1-phenylhydrazine (0.24 g, 2 mmol) in CH_2Cl_2 (30 mL), the red hexavanadate 3 slowly dissolved to give a dark blue-green solution. After stirring for 5 h at room temperature under argon, the solution was concentrated to 15 mL and layered with 15 mL of anhydrous diethyl ether. After standing for 3 days at 4 °C, blue needles of 6 were collected in 37.5% yield. Anal. Calcd for $C_{42}H_{94}N_2O_{19}V_6$: C, 40.8; H, 7.61; N, 2.27. Found: C, 40.7; H, 7.54; N, 2.20. IR (KBr pellet, cm^{-1}): 3452 (w), 2959 (m), 2865 (m), 1603 (w), 1482 (m), 1460 (m), 1386 (w), 1130 (m), 945 (vs), 750 (m), 605 (w), 565 (w), 480 (w), 400 (m). UV/vis [CH_2Cl_2; λ_{max}, nm (ϵ, cm^{-1} M^{-1})]: 243 (114000), 332 (2200), 786 (820).

Preparation of $[(n\text{-}C_4H_9)_4N]_2[V_6O_7(OH)_6\{(OCH_2)_3CCH_3\}_2]$ (7). Methylene chloride (30 mL) was added slowly with stirring to $[(n\text{-}C_4H_9)_4N]_2[V_6O_{13}\{(OCH_2)_3CCH_3\}_2]$ (3) (0.61 g, 0.5 mmol) and 1,2-diphenylhydrazine (0.28 g, 1.5 mmol), resulting in a dark green solution. After 10 h of stirring at room temperature, the solution turned dark

(15) Barrows, J. N.; Jameson, G. B.; Pope, M. T. *J. Am. Chem. Soc.* **1985**, *107*, 1771.

(16) $[(C_6H_5AsO_3)_2W_6O_{18}(OH)]^{3-}$: Wasfi, S. H.; Kwak, W.; Pope, M. T.; Barkigia, K. M.; Butcher, R. J.; Quicksall, C. O. *J. Am. Chem. Soc.* **1978**, *100*, 7786.

(17) $[SiV_3W_9O_{40}]^{7-}$: Finke, R. G.; Rapko, B.; Saxton, R. J.; Domaille, P. J. *J. Am. Chem. Soc.* **1986**, *108*, 2947.

(18) Newkome, G. R.; Baker, G. R. *Org. Prep. Proced. Int.* **1986**, *18*, 119.

(19) Newkome, G. R.; Yao, Z.; Baker, G. R.; Gupta, V. K. *J. Org. Chem.* **1985**, *50*, 2004.

Table I. Crystal Data for $[(C_4H_9)_4N]_2[V_6O_{13}\{(OCH_2)_3CR\}_2]$ (R = NO_2, **1**; CH_2OH, **2**·DMF; CH_3, **3**), $[V_6O_{11}(OH)_2\{(OCH_2)_3CCH_3\}_2]$·2DMF·$(C_2H_5)_2O$ (**5**·2DMF·$(C_2H_5)_2O$), $[(C_4H_9)_4N]_2[V_6O_9(OH)_4\{(OCH_2)_3CCH_3\}_2]$ (**6**), and $[(C_4H_9)_4N]_2[V_6O_7(OH)_6\{(OCH_2)_3CCH_3\}_2]$·$2CH_2Cl_2$·$0.5C_6H_5NNC_6H_5$ (**7**·$2CH_2Cl_2$·$0.5(C_6H_5N)_2$)

formula	**1** $C_{40}H_{84}N_4O_{23}V_6$	**2**·DMF $C_{42}H_{90}N_2O_{21}V_6$·DMF	**3** $C_{40}H_{90}N_2O_{19}V_6$	**5**·2DMF·$(C_2H_5)_2O$ $C_{20}H_{44}N_2O_{22}V_6$	**6** $C_{42}H_{92}N_2O_{19}V_6$	**7**·$2CH_2Cl_2$·$0.5C_6H_5NNC_6H_5$ $C_{42}H_{96}N_2O_{19}V_6$·$2CH_2Cl_2$·$0.5C_6H_5NNC_6H_5$
fw	1294.8	1337.9	1232.8	970.2	1234.8	1499.8
T, K	233	233	233	233	233	233
a, Å	11.470 (2)	12.003 (2)	11.460 (2)	10.362 (2)	11.534 (2)	13.613 (3)
b, Å	12.149 (2)	16.900 (3)	12.237 (2)	10.513 (3)	12.161 (3)	16.090 (4)
c, Å	12.433 (2)	16.769 (3)	12.331 (2)	10.366 (2)	12.483 (4)	16.077 (4)
α, deg	63.24 (1)	90.00	62.88 (1)	116.33 (1)	62.86 (2)	86.36 (1)
β, deg	63.45 (1)	106.95 (1)	63.50 (1)	93.56 (1)	63.15 (2)	80.71 (2)
γ, deg	79.31 (1)	90.00	77.52 (1)	62.40 (1)	78.87 (2)	80.46 (1)
V, Å^3	1383.5 (5)	3253.8 (11)	1377.4 (5)	882.2 (7)	1389.7 (7)	3424.1 (12)
space group	$P\bar{1}$	$P2_1/c$	$P\bar{1}$	$P\bar{1}$	$P\bar{1}$	$P\bar{1}$
Z	1	2	1	1	1	2
D_{calcd}, g cm^{-3}	1.55	1.37	1.49	1.83	1.48	1.45
μ(Mo Kα)	10.2	9.3	10.1	8.9	10.0	9.7
$R(F_o)$	0.049	0.054	0.055	0.043	0.043	0.042
$R_w(F_o)$	0.062	0.060	0.059	0.049	0.045	0.049

brown, whereupon it was concentrated to 10 mL and layered with 15 mL of diethyl ether. After standing for 1 week at 4 °C, brown block-shaped crystals of **7**·$2CH_2Cl_2$·$0.5C_6H_5NNC_6H_5$ were collected in 20% yield. Anal. Calcd for $C_{50}H_{105}N_3O_{19}Cl_4V_6$: C, 42.0; H, 7.35; N, 2.94. Found: C, 41.8; H, 7.29; N, 2.90. IR (KBr pellet, cm^{-1}): 3450 (w), 2959 (m), 2865 (m), 1475 (m), 1450 (m), 1378 (w), 1122 (m), 1042 (s), 938 (vs), 595 (w), 473 (w), 380 (m). UV/vis [CH_2Cl_2; λ_{max}, nm (ϵ, cm^{-1} M^{-1})]: 238 (21 000), 301 (20 000), 440 (570), 874 (250).

^{17}O Nuclear Magnetic Resonance Spectra. A. Sample Preparation. Samples were prepared by using 30% ^{17}O enriched water, purchased from Cambridge Chemicals. All preparative procedures involving ^{17}O-enriched water were carried out in closed systems in order to prevent isotopic dilution by atmospheric water. The ^{17}O-enriched sample of $[(n\text{-}C_4H_9)_4N]_3[H_3V_{10}O_{28}]$ was prepared by the method of Day, Klemperer, and Maltbie.[7] ^{17}O-enriched samples of the polyhydroxylic-derived complexes were prepared by adjusting the conditions described above in order to minimize isotopic dilution by atmospheric oxygen. Preparations were generally carried out on a 0.50-g scale.

B. Spectral Measurements. ^{17}O NMR spectra were recorded at 297 K at 40.66 MHz by using the pulse FT NMR technique on the Varian XL-300 spectrometer interfaced with a Motorola 68000 microprocessor computer. The spectra were digitized by using 1600, 4160, 6976, or 8000 data points depending on the acquisition times and spectral bandwidths employed. The pulse width used for a 90° pulse was 25 μm. Deuteriated dichloromethane and acetonitrile were employed as internal locks. Spectra were obtained by using a double-precision acquisition technique in cylindrical 10-mm-o.d. sample tubes (3.0-mL sample volume) and referenced for internal $H_2{}^{17}O$. Chemical shifts are reported in parts per million with positive values in the low-field direction relative to $H_2{}^{17}O$. All chemical shifts and line width data were reproducible within ±2% and ±5%, respectively. Since the integrated intensities of ^{17}O NMR resonances are only a qualitative measure of relative numbers of oxygen nuclei, spin quantitations were not performed on the various spectra. The major contributing factors to this unreliability of intensity data include variations in relaxation rates for nonequivalent oxygens, decreases in RF pulse power with increasing frequency from the carrier, the decreases in signal intensity by audio frequency filtering.[24,25] Thus, chemical shift data have been used to provide structural information.[24]

C. Spectral Parameters. For the complexes of this study the following parameters or ranges were employed: number of transients, 69 930; acquisition time, 50 ms; survey width, 80 000 Hz; transmitter offset, 20 000 Hz; exponential line broadening, 10 Hz.

EPR Methods. EPR samples of the hexavanadate complex were prepared in freshly distilled DMF at 1 and 5 mM concentrations by electrochemical reduction under an inert argon atmosphere. Samples of approximately 1-mL volume were transferred and frozen under inert atmosphere by plunging large 9-mm-o.d., 7-mm-i.d. quartz sample tubes into liquid nitrogen.

The EPR[20] system was a Bruker ER-420 spectrometer modified for superheterodyne operation and for pulsed, saturation recovery T_1 measurements[21a] and pulse field-sweep EPR.[21b] The cryogenic system consisted of a set of double dewars, and the EPR cavity and field modulation coils were contained within the inner dewar. For stabilizing temperature between the temperatures of liquid helium (4.2 K) and liquid nitrogen (77 K), a previously described heater-feedback control system was used.[21] Absorption derivative ($d\chi''/dH$) EPR spectra were obtained with 100-kHz field modulation of approximately 4 G peak-to-peak (an amplitude much less than the line width of the EPR signals). Repetitive spectral sweeps over a 2000-G range, centered at $g = 2.00$, were collected in the memory of a Tracor 570 signal averager and stored for future manipulation in the memory of a microcomputer. The microwave frequency was measured to four significant figures by a wave meter which had been calibrated vs an XL Microwave Model 3120 frequency counter. The magnetic field was calibrated by a Harvey-Wells G-502 gaussmeter. A 1 mM $[Cu(H_2O)_6]^{2+}$ sample in pH 1.5 $NaClO_4$ was used as a standard in comparing integrated intensities. Since our EPR system is designed for pulse and ENDOR measurements rather than precise spin quantitations, we accept 50% uncertainty in spin quantitation. EPR simulations used the QPOWA routine.[22,23]

X-ray Crystallographic Studies. The details of the crystal data, data collection methods, and refinement procedures are summarized in Table I and the supplementary tables. In all cases, data were collected at −40 °C at scan speeds of 1–15° min^{-1}. The refinements of the V(V) clusters, **1**–**3**, proved unexceptional. Some disorder of the terminal carbon atoms of the cations was apparent in the large thermal parameters associated with these atoms. No further attempts to model the disorder were introduced.

A check of the unit cell dimensions revealed that using relaxed constraints for **5** converts the triclinic cell into C-centered monoclinic or F-centered orthorhombic cells. However, a check of reflection intensities did not reveal the required equivalences, nor did long-exposure axial photographs reveal any signs of superlattice conditions.

In the case of $[(n\text{-}C_4H_9)_4N]_2[V_6O_9(OH)_4\{(OCH_2C)_3CCH_3\}_2]$ (**6**), the hydrogen positions were located from the difference Fourier maps. After full-matrix least-squares refinement cycles using anisotropic thermal parameters for all non-hydrogen atoms of the anion and the cation and fixed isotropic temperature factors for the hydrogen atoms of the cation (positioned at idealized C–H distances of 0.96 Å), a difference Fourier synthesis exhibited electron density maxima located at positions consistent with O2 and O6 as the protonation sites. The locations of the hydrogen atoms were confirmed by high-angle ($2\theta > 37°$) refinement of the non-hydrogen atoms followed by difference Fourier synthesis based on inner shell data. This procedure clearly revealed all but three hydrogen atoms of the cation and all hydrogen atoms of the anion. Hydrogen atoms bonded to O2 and O6 were included in the structural model and refined as independent isotropic atoms in the final least-squares cycles.

The protonation sites on $[(n\text{-}C_4H_9)_4N]_2[V_6O_7(OH)_6\{(OCH_2)_3CCH_3\}_2]$·$2CH_2Cl_2$·$0.5C_6H_5NNC_6H_5$ (**7**·$2CH_2Cl_2$·$0.5C_6H_5NNC_6H_5$) were also apparent on the difference Fourier maps calculated on the basis of anisotropic refinement of all non-hydrogen atoms of the cation and anion. The hydrogen atom positions were again confirmed by high-angle refinement of non-hydrogen atoms, followed by difference Fourier synthesis of the inner shell data.

Upon full-matrix least-squares refinement using anisotropic temperature factors for all non-hydrogen atoms of **5**, all hydrogen atom positions

(20) Abbreviations: EPR, electron paramagnetic resonance; T_1, spin–lattice relation time; μW, microwatt; G, gauss, χ'', absorptive part of the complex magnetic susceptibility; o.d., outside diameter; i.d., inside diameter.

(21) (a) Scholes, C. P.; Janakiraman, R.; Taylor, H.; King, T. E. *Biophys. J.* **1984**, *45*, 1027. (b) Falkowski, K. M.; Scholes, C. P.; Taylor, H. *J. Magn. Reson.* **1986**, *68*, 453.

(22) (a) Nilges, M. J. Ph.D. Thesis, University of Illinois, Urbana, Illinois, 1979. (b) Belford, R. L.; Nilges, M. J. *Computer Simulation of Powder Spectra*, EPR Symposium, 21st Rocky Mountain Conference, Denver, CO, 1979.

(23) Maurice, A. M. Ph.D. Thesis, University of Illinois, Urbana, Illinois, 1980.

(24) Klemperer, W. G. *Angew. Chem., Int. Ed. Engl.* **1978**, *17*, 246.

(25) Filowitz, M.; Ho, R. K. C.; Klemperer, W. G.; Shum, W. *Inorg. Chem.* **1979**, *18*, 93.

were clearly visible on the difference Fourier map. The ligand and solvent hydrogen atoms were introduced as fixed contributors at idealized positions, and several cycles of full-matrix least-squares refinement were performed to give an R of 0.047 upon convergence of this model. The Fourier map clearly revealed an excursion of electron density consistent with protonation of O3. Introduction of this H-atom location and refinement of its positional parameters and isotropic temperature factor resulted in convergence of the structural model at $R = 0.043$.

Results and Discussion

Preparation and Spectroscopic Characterization of the Complexes. The complex $[(n\text{-}C_4H_9)_4N]_3[H_3V_{10}O_{28}]$ provides a convenient starting point for the synthesis of polyoxovanadate coordination complexes in aprotic, polar solvents. The reactions of $[(n\text{-}C_4H_9)_4N]_3[H_3V_{10}O_{28}]$ with tris(hydroxymethyl)methane derivatives, $(HOCH_2)_3CR$ (R = NO_2, CH_2OH, CH_3, NMe_2), in acetonitrile yield upon recrystallization lustrous red crystals of $[(n\text{-}C_4H_9)_4N]_2[V_6O_{13}\{(OCH_2)_3CR\}_2]$ in 40–50% yield, depending upon the identity of R. The stoichiometry of the reaction under optimal conditions conforms to the following equation:

$$2(TBA)_3[H_3V_{10}O_{28}] + 6(HOCH_2)_3CR \rightarrow 3(TBA)_2[V_6O_{13}\{(OCH_2)_3CR\}_2] + 12H_2O + V_2O_5$$

The identity of the insoluble white powder V_2O_5, produced as a side product of the reaction, was confirmed by infrared spectroscopy. The crystalline products are indefinitely stable when exposed to the atmosphere, while solutions of the complexes decompose over a period of days when exposed to the atmosphere at room temperature. The infrared spectra of the complexes exhibit characteristic features in the 790–970-cm^{-1} range, attributed to $\nu(V{=}O_t)$ and $\nu(V{-}O{-}V)$, and a feature in the 1000–1050-cm^{-1} region assigned to $\nu(C{-}O)$ of the ligands.

The ^{17}O NMR spectra of these complexes, measured in CD_3CN solutions, display three completely resolved signals, as shown in Figure 1 for $[(n\text{-}C_4H_9)_4N]_2[V_6O_{13}\{(OCH_2)_3CCH_3\}_2]$. The resonances may be assigned on the basis of the general correlation between chemical shift and the π-bond order of the V–O bond, which increases with decreasing bond order.[24,25] The signal at 1207 ppm is assigned to the terminal oxo groups, while the bridging oxo groups appear at 885 ppm and the central oxo group appears at 21 ppm. The alkoxy oxygen atoms do not exchange with ^{17}O oxo groups and hence are not enriched or observed.[5k,25]

The ^{17}O NMR spectrum of the neutral, protonated complex $[V_6O_{11}(OH)_2\{(OCH_2)_3CCH_3\}_2]$ (**5**) shown in Figure 1b is similar to that of the parent compound **3** with the exception of a new resonance appearing at 331 ppm assigned to the doubly bridging OH groups.

Samples of $[V_6O_{11}(OH)_2\{(OCH_2)_3CCH_3\}_2$ (**5**) may also be selectively ^{17}O-enriched since the complex exchanges oxygen with water slowly at room temperature. Thus, upon treatment of **5** with 5 equiv of $H_2{}^{17}O$ at 40 °C, the ^{17}O spectrum shown in Figure 1c is observed. Comparison of this spectrum with that of the statistically ^{17}O-enriched complex of Figure 1b reveals that the selectively enriched species has been preferentially enriched at the hydroxylic sites $\{V_2{-}OH\}$ in the $\{V_6O_{19}\}$ framework. Other site-selective oxygen-exchange processes have been observed for $[Ta_6O_{19}]^{8-}$ [26] and $[H_3V_{10}O_{28}]^{3-}$.[7] It should be noted that the related hexavanadate species $[Rh(C_5Me_5)]_4[V_6O_{19}]$ [14a] also displays site-selective oxygen exchange at the analogous bridging oxygen sites of the $\{V_2{-}O{-}Rh\}$ type.

The hexavanadate clusters $[V_6O_{13}\{(OCH_2)_3CR\}_2]^{2-}$ exhibit metal sites which correspond grossly to mononuclear VOL_5 species with the vanadate centers in approximately tetragonal sites with a single terminal oxo group (vide infra). As such, these species may be classified as type I polyoxoanions[27] and are expected to exhibit well-behaved reduction processes, in common with other hexametalate species.[28] As anticipated, the complexes undergo

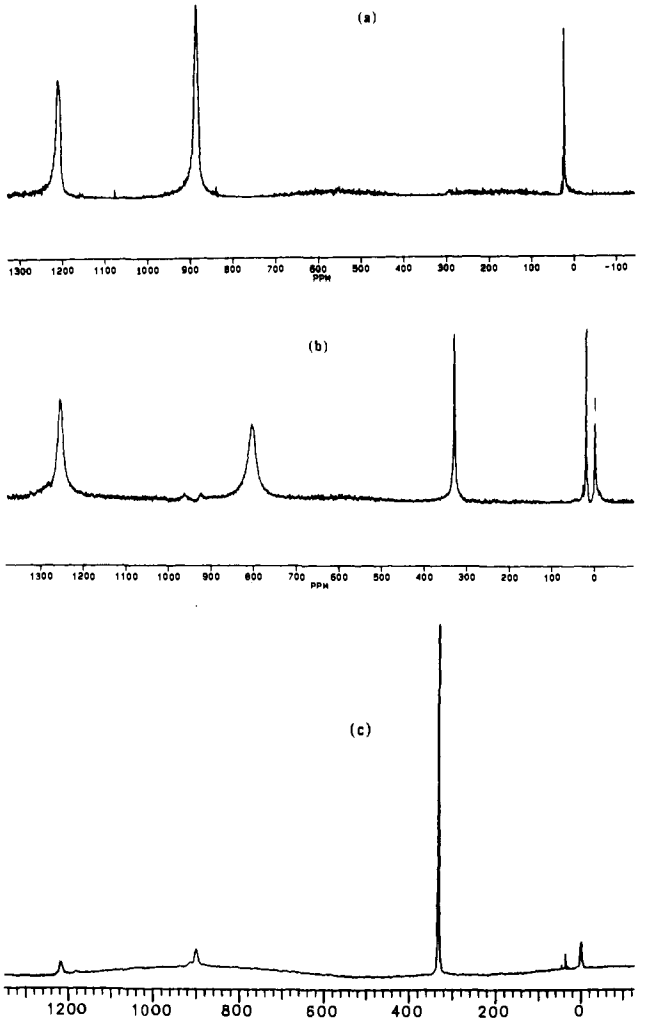

Figure 1. (a) ^{17}O NMR spectrum of statistically enriched $[(n\text{-}C_4H_9)_4N]_2[V_6O_{13}\{(OCH_2)_3CCH_3\}_2]$ in CD_3CN. (b) ^{17}O NMR spectrum of statistically enriched $[V_6O_{11}(OH)_2\{(OCH_2)_3CCH_3\}_2]$ in CD_3CN. (c) ^{17}O NMR spectrum of selectively enriched $[V_6O_{11}(OH)_2\{(OCH_2)_3CCH_3\}_2]$ in CD_3CN.

reversible one-electron reductions at potentials in the −0.65 to −1.20 V range, as measured by cyclic voltammetry and discussed below. In contrast, attempts at chemical reduction using organohydrazine reagents as reducing agents resulted in both reduction and proton transfer to yield both a mixed valence V(V)/V(IV) species with mixed oxo and hydroxy bridging and a fully reduced V(IV) hydroxy-bridged species.

Addition of 2 equiv of 1-methyl-1-phenylhydrazine to $[(n\text{-}C_4H_9)_4N]_2[V_6O_{13}\{(OCH_2)_3CCH_3\}_2]$ in acetonitrile results in an immediate color change from the characteristic red of solutions of the polyoxovanadate(V) to a deep blue. Upon addition of diethyl ether to this solution, brilliant blue crystals of the air-sensitive $[(n\text{-}C_4H_9)_4N]_2[V_6O_9(OH)_4\{(OCH_2)_3CCH_3\}_2]$ (**6**) are isolated. Addition of larger amounts of reductant causes solutions of this mixed valence species $[V^V{}_2V^{IV}{}_4O_9(OH)_4\{(OCH_2)_3CCH_3\}_2]^{2-}$ slowly to discharge their characteristic blue color to give a brown solution. By employing 1,2-diphenylhydrazine as the reductant, we were able to isolate brown crystals of the fully reduced species $[(n\text{-}C_4H_9)_4N]_2[V_6O_7(OH)_6\{(OCH_2)_3CCH_3\}_2]\cdot 2CH_2Cl_2\cdot 0.5C_6H_5NNC_6H_5$. In these reactions, the organohydrazines serve both as reductant and as proton sources, according to the equations below:

$$[V_6O_{13}\{(OCH_2)_3CCH_3\}_2]^{2-} + 4H_2NNMePh \rightarrow [V_6O_9(OH)_4\{(OCH_2)_3CCH_3\}_2]^{2-} + 4HNMePh + 2N_2$$

$$[V_6O_{13}\{(OCH_2)_3CCH_3\}_2]^{2-} + 3HPhNNHPh \rightarrow [V_6O_7(OH)_6\{(OCH_2)_3CCH_3\}_2]^{2-} + 3PhNNPh$$

(26) Chisholm. M. H.; Folting, K.; Hoffman, J. C.; Kirkpatrick, C. C. *Inorg. Chem.* **1984**, *23*, 1021.
(27) Pope, M. T. *Inorg. Chem.* **1972**, *11*, 1973.
(28) (a) Harmalker, S. P.; Leparulo, M. A.; Pope, M. T. *J. Am. Chem. Soc.* **1983**, *105*, 4286. (b) So, H.; Lee, C. W. *Bull. Korean Chem. Soc.* **1990**, *11*, 115 and references therein.

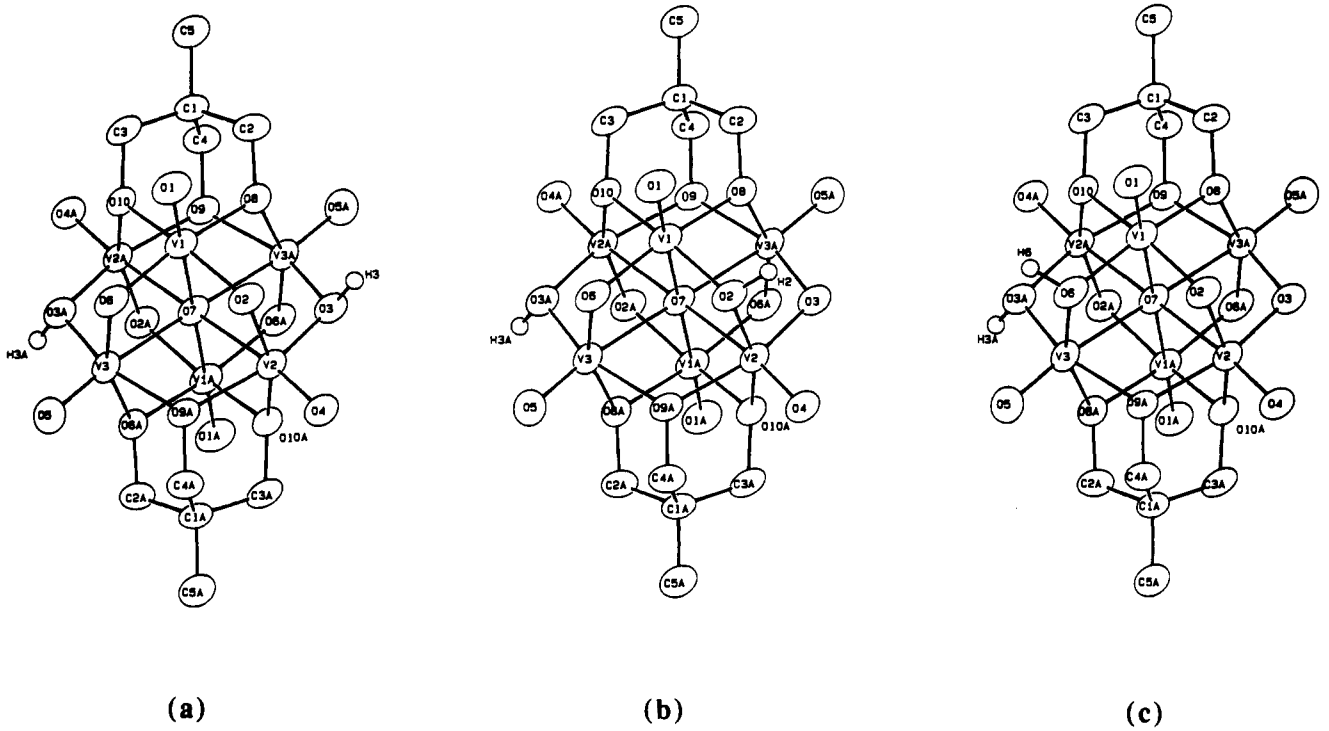

(a) (b) (c)

Figure 2. Possible geometric isomers for $[V_6O_{11}(OH)_2\{(OCH_2)_3CCH_3\}_2]$, arising from different protonation patterns.

The optimal conditions for reduction of $[V_6O_{13}\{(OCH_2)_3CCH_3\}_2]^{2-}$ to $[V_6O_9(OH)_4\{(OCH_2)_3CCH_3\}_2]^{2-}$ require the addition of 4 rather than 2 equiv of 1-methyl-1-phenylhydrazine. The major organic product of the coupled reduction/protonation process has been identified as *N*-methylaniline by NMR, indicating the overall stoichiometry shown above. On the other hand, the complex may be fully reduced by the addition of 3 equiv of 1,2-diphenylhydrazine, with the production of azobenzene, which is observed both in the crystal structure of the material as a molecule of crystallization and in the NMR spectrum of the product mixture in solution.

Attempts to isolate crystals of the two-electron, two-proton product $[V_6O_{11}(OH)_2\{(OCH_2)_3Cr\}_2]^{2-}$ proved unsuccessful. Reaction of $[V_6O_{13}\{(OCH_2)_3CCH_3\}_2]^{2-}$ (**3**) with 2 equiv of 1-methyl-1-phenylhydrazine initially produces a green-brown solution whose electronic spectrum is identical to that of the electrochemically generated $[V_6O_{11}(OH)_2\{(OCH_2)_3CCH_3\}_2]^{2-}$ (vide infra). However, upon standing for several hours, the characteristic green color is discharged and the solution turns blue-violet. A mixture of red crystals of $(TBA)_2[V_6O_{13}\{(OCH_2)_3CCH_3\}_2]$ (**3**) and blue crystals of $(TBA)_2[V_6O_9(OH)_4\{(OCH_2)_3CCH_3\}_2]$ (**6**) is isolated from this solution upon addition of ether, suggesting that while $[V_6O_{11}(OH)_2\{(OCH_2)_3CCH_3\}_2]^{2-}$ is formed initially, this species is unstable with respect to disproportionation into the fully oxidized **3** and the four-electron, four-proton product **6**.

$$[V_6O_{13}\{(OCH_2)_3CCH_3\}_2]^{2-} + 2MePhNNH_2 \rightarrow [V_6O_{11}(OH)_2\{(OCH_2)_3CCH_3\}_2]^{2-} + 2HNMePh + N_2$$

$$2[V_6O_{11}(OH)_2\{(OCH_2)_3CCH_3\}_2]^{2-} \rightarrow [V_6O_{13}\{(OCH_2)_3CCH_3\}_2]^{2-} + [V_6O_9(OH)_4\{(OCH_2)_3CCH_3\}_2]^{2-}$$

Reduction and protonation processes may be decoupled as illustrated by the synthesis of the neutral polyoxometalate species $[V_6O_9(OH)_2\{(CH_2O)_3CCH_3\}_2]$ (**5**). Thus, the reaction of **3** with 2 equiv of $HBF_4\cdot(C_2H_5)_2O$ yields **5** in nearly quantitative yield. The infrared spectrum of **5** is similar to that of **3** with the exception of the absence of the medium intensity feature at 816 cm^{-1}. A band at 810–820 cm^{-1} is characteristic of the $(TBA)_2[V_6O_{13}\{(OCH_2)_3CR\}_2]$ species **1–4** and is most likely associated with a V–O–V group vibration. Protonation of two bridging oxo groups in **5** shifts this band to 796 cm^{-1}, while in the four-electron-reduced, four-hydroxy-bridged species **6** a medium intensity feature at 750 cm^{-1} may be associated with ν(V–O–V). The band is totally absent in the spectrum of **7**, which is essentially featureless in the 600–900-cm^{-1} region.

The infrared evidence indicates protonation of doubly bridging oxo sites, an observation consistent with the greater nucleophilicity/basicity of bridging oxo groups relative to terminal oxo groups and with the X-ray data discussed below. Protonation of doubly bridging oxo groups has been established for $[H_2V_{10}O_{28}]^{4-}$ [29] and $[H_4PV_{14}O_{42}]^{5-}$.[30] Analogous patterns of behavior have been established for $[Nb_2W_4O_{19}]^{4-}$,[13j] $[V_2W_4O_{19}]^{4-}$,[31] $[SiV_3W_9O_{40}]^{7-}$,[17] and $[Mo_{12}PO_{40}]^{2-}$ [32] where doubly bridging oxo groups are more nucleophilic/basic than terminal oxo groups.

Since the girdle of six doubly bridging oxo groups at the $[V_6O_{13}\{(OCH_2)_3CR\}_2]^{2-}$ core provides potential protonation sites, three isomers are possible for a doubly protonated core $[V_6O_{11}(OH)_2\{(OCH_2)_3CR\}_2]$, identified in parts a, b, and c of Figure 2. The X-ray structure of **5** is consistent with a single isomer in the solid state. The ^{17}O NMR spectrum of **5** is likewise consistent with a single symmetrically substituted isomer.

The $[V_6O_{13}\{(OCH_2)_3CR\}_2]^{2-}$ anion reacts similarly with silylating reagents to yield the derivatives $[V_6O_{11}(OR')_2\{(OCH_2)_3CR\}_2]$.

$$[V_6O_{13}\{(OCH_2)_3CR\}_2]^{2-} \xrightarrow[-X^-]{+R'X} [V_6O_{11}(OR')_2\{(OCH_2)_3CR\}_2]$$

5, R′ = H, X = BF_4^-

5a, R′ = $Si(CH_3)_2[C(CH_3)_3]$, X = $CF_3SO_3^-$

5b, R′ = $Si(CH_3)_3$, X = Cl^-

The infrared spectra of the silylated derivatives are similar to those of the oxidized complexes **1–4** with the exception of the absence of the 810–820-cm^{-1} feature and the appearance of a very strong absorbance at 790 cm^{-1}, characteristic of ν(Si–C). The ^{29}Si NMR spectrum of **5a** displays a single resonance at 16.9 ppm relative to tetramethylsilane. Similarly, the ^{13}C NMR spectrum of **5a** showed only three resonances at 25.90, 20.59, and −2.15

(29) Capparelli, M. V.; Goodgame, D. M. L.; Hayman, P. B.; Skapski, A. C. *J. Chem. Soc., Chem. Commun.* **1986**, 776.
(30) Khan, M. I.; Zubieta, J.; Toscano, P. Unpublished results.
(31) Kemperer, W. G.; Shum, W. *J. Am. Chem. Soc.* **1978**, *100*, 4891.
(32) Knoth, W. M.; Harlow, R. C. *J. Am. Chem. Soc.* **1981**, *103*, 4265.

Table II. Absorption Spectral Data for Hexavanadate Complexes

complex	solvent	λ_{max}, nm (ϵ_M)[a]
$(TBA)_2[V_6O_{13}\{(OCH_2)_3CR\}_2]$[b]		
R = NO_2 (**1**)	DMF	274 (7400), 384 (2500)
R = CH_2OH (**2**)	DMF	275 (14000), 357 (6500)
R = CH_3 (**3**)	DMF	275 (13000), 338 (6100)
	CH_2Cl_2	246 (17000), 359 (5400)
R = CH_2CH_3 (**3a**)	DMF	270 (12000), 340 (5500)
R = NMe_2 (**4**)	DMF	275 (12000), 342 (6300)
R = $CH_2C_6H_5$ (**4a**)	DMF	270 (12500), 360 (5200)
$[V_6O_{11}(OH)_2\{(OCH_2)_3CCH_3\}_2]$ (**5**)	DMF	265 (13000), 320 (sh)
$(TBA)_2[V_6O_9(OH)_4\{(OCH_2)_3CCH_3\}_2]$ (**6**)	DMF	273 (14000), 340 (5400), 785 (820)
	CH_2Cl_2	243 (14000), 332 (2200), 786 (230)
$(TBA)_2[V_6O_7(OH)_6\{(OCH_2)_3CCH_3\}_2]\cdot C_6H_5NNC_6H_5$ (**7**)	CH_2Cl_2	238 (19000), 301 (22000), 440 (570), 874 (250)
$[V_6O_{13}\{(OCH_2)_3CCH_3\}_2]^{3-}$ (**3b**)	CH_2Cl_2	247 (15000), 302 (7600), 784 (210)
$[V_6O_{11}(OH)_2\{(OCH_2)_3CCH_3\}_2]^{2-}$ (**5c**)	CH_3CN[c]	270 (15000), 320 (sh), 780 (385)
	CH_2Cl_2[d]	250 (16000), 310 (sh), 782 (410)

[a] Extinction coefficients are approximate values. [b] TBA ≡ $[(n\text{-}C_4H_9)_4N]^+$. [c] Produced by the electrochemical reduction of $[V_6O_{11}(OH)_2\{(OCH_2)_3CCH_3\}_2]$ (**5**). [d] Produced by the reaction of $[V_6O_{13}\{(OCH32)_3CCH_3\}_2]^{2-}$ (**3**) with $H_2NNMePh$.

Table III. Voltammetric Parameters for the Redox Processes of the Complexes of This Study[a]

compound[b]	$E_{1/2}$, V[c]	$E_p^f - E_p^r$, mV	(i_p^f/i_p^r)	$i_p/Cv^{1/2}$, mA $s^{1/2}$ $mV^{-1/2}$ M^{-1}[d]	n_{app}[e]
$(TBA)_2[V_6O_{13}\{(OCH_2)_3CNO_2\}_2]$ (**1**)	−0.67	61	1.0	9.1	1.0
$(TBA)_2[V_6O_{13}\{(OCH_2)_3CCH_2OH\}_2]$ (**2**)	−0.76	60	1.0	9.2	1.0
$(TBA)_2[V_6O_{13}\{(OCH_2)_3CCH_3\}_2]$ (**3**)	−1.20	62	1.0	8.8	1.0
$(TBA)_2[V_6O_{13}\{(OCH_2)_3CCH_2CH_3\}_2]$ (**3a**)	−1.17	72	1.0	8.5	1.0
$(TBA)_2[V_6O_{13}\{(OCH_2)_3CCH_2C_6H_5\}_2]$ (**4a**)	−0.85	67	1.0	8.7	1.0
$(TBA)_2[V_6O_{13}\{(OCH_2)_3CNMe_2\}_2]$ (**4**)	−1.18	77	1.2	7.7	0.8
$(TBA)_2[V_6O_{11}(OH)_2\{(OCH_2)_3CCH_3\}_2$ (**5c**)	−0.09	102	1.3	8.1	1.0
$(TBA)_2[V_6O_9(OH)_4\{(OCH_2)_3CCH_3\}_2]$ (**6**)	−0.31	87	1.2	8.2	1.0
$(TBA)_2[V_6O_7(OH)_6\{(OCH_2)_3CCH_3\}_2]$ (**7**)	−0.95	69	1.0	8.5	1.0
	−1.72	74	1.2	7.9	1.0
$[V_6O_{11}(OH)_2\{(OCH_2)_3CCH_3\}_2]$ (**5**)	−0.69	93	1.0	10.4	1.9

[a] At a platinum bead working electrode, using solutions 1.0×10^{-3} M in complex in 0.1 M $(Bu_4N)PF_6$ in acetonitrile or *N*,*N*-dimethylformamide. All potentials are referred to the ferrocene/ferrocenium couple. Cyclic voltammograms were obtained at sweep rates of 200 mV s^{-1}. [b] TBA ≡ $[(n\text{-}C_4H_9)_4N]^+$. [c] Estimated from $E_{1/2} = (E_p^f - E_p^4)/2 \sim E_p^f - 29$ mV. The shape parameter $E_p^f - E_p^r$ lay within the range 60–80 mV for all couples except that of **5c**. [d] The current function for the ferrocene/ferrocenium couple at the same electrode is 9.2 mA $s^{1/2}$ $mV^{-1/2}$ M^{-1}. [e] The value of *n* (number of electrons) was determined by controlled-potential electrolysis at a potential 0.2 V from the process of interest.

ppm from tetramethylsilane, consistent with one $SiMe_2Bu^t$ environment and hence a single, symmetrically substituted geometric isomer of **5a**.

The electronic absorption spectral data for the complexes are summarized in Table II. All the hexavanadates, whether fully oxidized, mixed valence, or fully reduced, exhibit two intense bands in the near-ultraviolet region (240–390 nm) which are ascribed to oxygen-to-metal charge-transfer transitions. The solvent dependence of the positions of these features is consistent with their assignment as charge-transfer bands. The spectra of the oxidized clusters **1–5** are characterized by the presence of the two charge-transfer bands exclusively. Upon reduction of the polyanions, new bands appear in the visible region. In the partially reduced species $[V^V_5V^{IV}O_{13}\{(OCH_2)_3CCH_3\}_2]^{3-}$ (**3b**), $[V^V_4V^{IV}_2O_{11}(OH)_2\{(OCH_2)_3CCH_3\}_2]^{2-}$ (**5c**), and $[V^V_2V^{IV}_4O_9(OH)_4\{(OCH_2)_3CCH_3\}_2]^{2-}$ (**6**), the new band appears in the 780–815-nm range and is assigned as an intervalence charge-transfer (IVCT) band, V(IV) → V(V). The magnitude of the extinction coefficients is roughly proportional to the number of d^1 sites associated with the cluster with a value of ca. 200/V(IV). While Keggin anion heteropoly blue species generally exhibit two IVCT bands,[33] the hexametalate cores $[M_6O_{19}]^{n-}$ (M = Mo, W) have been reported to have a single transition of this type.[34] The reduced hexavanadate species of this study appear to conform to this general trend. The intensities of the IVCT bands of the hexavanadate series are also consistent with values observed for other hexametalate species which exhibit molar extinction coefficients in the range of 280/reduced site.

The fully reduced species $[V^{IV}_6O_7(OH)_6\{(OCH_2)_3CCH_3\}_2]^{2-}$ (**7**) shows two bands in the visible region at 440 and 874 nm with molar extinction coefficients of 570 and 250 cm^{-1} M^{-1}, respectively.

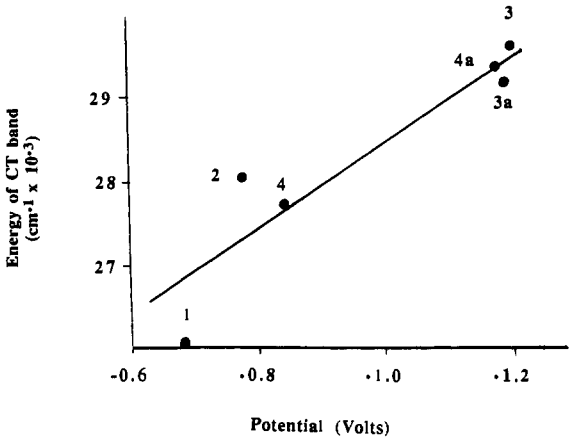

Figure 3. Plot of reduction potential vs the lowest energy charge-transfer band for $[V_6O_{13}\{(OCH_2)_3CR\}_2]^{2-}$ complexes. The labels refer to the numbering scheme used in the text.

These are most likely ligand field transitions, which, on the basis of approximate C_{4v} symmetry of the V(IV) sites, would correspond to $b_2 \rightarrow e$ and $b_2 \rightarrow b$ excitations, that is, d_{xy} to $d_{xy,yz}$ and d_{xy} to $d_{x^2-y^2}$, respectively.[35,36]

Electrochemical Studies. The relevant electrochemical data for the hexavanadates of this study are summarized in Table III. The cyclic voltammograms of the oxidized clusters **1–4** at a platinum bead electrode in 0.1 M (TBA)PF_6/acetonitrile or (TBA)PF_6/DMF show a single one-electron reversible reduction at moderately negative potentials with respect to ferrocene/ferrocenium. The

(33) Varga, G. M., Jr.; Papaconstantinou, E.; Pope, M. T. *Inorg. Chem.* **1970**, *9*, 662.
(34) Che, M.; Fournier, M.; Launay, J. P. *J. Chem. Phys.* **1979**, *71*, 1954.
(35) Pope, M. T. *Inorg. Chem.* **1972**, *11*, 1973.
(36) Brown, D. B., Ed. *Mixed-Valence Compounds*; D. Reidel: Dordrecht, 1980; p 365.

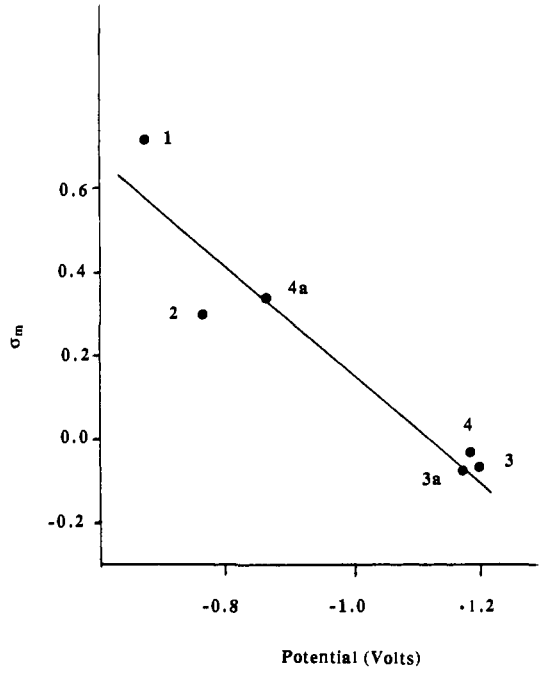

Figure 4. Plot of reduction potential vs Hammett σ_m constant for $[V_6O_{13}\{(OCH_2)_3CR\}_2]^{2-}$ complexes.

processes are judged electrochemically reversible on the basis of the ratio of peak heights for the cathodic and anodic processes and the peak-to-peak separations. The reduction potentials of complexes **1**–**4** correlate reasonably well with the energies of the lowest energy charge-transfer bands of the complexes, as illustrated by Figure 3. This observation is consistent with a model in which electrons added to a polyanion upon reduction enter the same metal orbitals that receive electron density in the oxygen-to-metal charge-transfer transitions.[37]

The substituent R of the triol ligand $[RC(CH_2O)_3]^{3-}$ produces a significant effect on the potential of the reduction. The variations in the half-wave potentials for the couple shown correlate with the Hammett σ_m constant,[38,39] as illustrated in Figure 4. The

$$[V^{V}_6O_{13}\{(OCH_2)_3CR\}_2]^{2-} \xrightleftharpoons{1e^-} [V^{V}_5V^{IV}O_{13}\{(OCH_2)_3CR\}_2]^{3-}$$

plot of $E_{1/2}$ vs σ_m exhibits nearly linear correlation, although, as previous authors have pointed out, the inadequacy of the σ_m values in this context must be borne in mind.[40] The trend is related to the electron density at the oxygen donors and suggests a largely inductive substituent effect. As expected, the electron-withdrawing NO_2 groups tend to stabilize the reduced cluster whereas electron density at the oxygen donors of the ligands with $R = CH_3$ is at a maximum for this series, and consequently the reduced form is destabilized.

The consequences of protonation of the oxidized species to give $[V_6O_{11}(OH)_2\{(OCH_2)_3CCH_3\}_2]$ (**5**) on the potential of the reduction process are significant. As expected, from electrostatic arguments, the neutral complex **5** is significantly more readily reduced than the anionic cluster **3**, as reflected in a reduction potential 0.51 V more positive for **5** compared to **3**. The cyclic voltammetry for **5** shows a quasi-reversible reduction. Although the peak height ratio $i_p^{ox}/i_p^{r}{}_{ed}$ approaches 1.0 at 200 mV/s, the peak-to-peak separation ΔE_p increases with increasing sweep rate, consistent with a quasi-reversible process characterized by slow electron transfer. The one-electron reduction product of **5** is unstable as suggested by the deviation of the peak current ratio from unity at slower scan rates, while concomitantly the peak current function $i_p^{red}\nu^{1/2}$ approaches that for an overall two-electron reduction. Controlled potential electrolysis of **5** at −0.50 V results in a color change from the red characteristic of **5** to deep green-brown after complete electrolysis with the consumption of 2 faradays mol^{-1}. Examination of the catholyte by CV after the two-electron reduction indicated that a single major product,

$$[V^{V}_6O_{11}(OH)_2\{(OCH_2)_3CCH_3\}_2] \xrightleftharpoons{2e^-} [V^{V}_4V^{IV}_2O_{11}(OH)_2\{(OCH_2)_3CCH_3\}_2]^{2-}$$

characterized by a quasi-reversible one-electron oxidation at −0.09 V, had been formed. The electronic spectrum of the reduction product was identical to that of $[V_6O_{11}(OH)_2\{(OCH_2)_3CCH_3\}_2]^{2-}$ produced by reaction of $[V_6O_{13}\{(OCH_2)_3CCH_3\}_2]^{2-}$ with $H_2NNMePh$. The electrochemically generated solution of $[V_6O_{11}(OH)_2\{(OCH_2)_3CCH_3\}_2]^{2-}$ was observed to disproportionate over several hours to give a mixture of **3** and **6**.

The mixed-valence complex $[V_6O_9(OH)_4\{(OCH_2)_3CCH_3\}_2]^{2-}$ (**6**) possesses a CV characterized by a single quasi-reversible one-electron oxidation with $E_{1/2}$ of −0.32 V, while the fully reduced species $[V_6O_7(OH)_6\{(OCH_2)_3CCH_3\}_2]^{2-}$ (**7**) exhibits a reversible one-electron oxidation at −0.95 V. Thus, the relative ease of oxidation of the reduced clusters $[V^{V}_4V^{VI}_2O_{11}(OH)_2\{(OCH_2)_3CCH_3\}_2]^{2-}$, $[V^{V}_2V^{VI}_4O_9(OH)_4\{(OCH_2)_3CCH_3\}_2]^{2-}$, and $[V^{IV}_6O_7(OH)_6\{(OCH_2)_3CCH_3\}_2]^{2-}$ correlates with the number of reduced V(IV) centers associated with the cluster.

$$[V_6O_{13-n}(OH)_n\{(OCH_2)_3CCH_3\}_2]^{2-} \rightleftharpoons [V_6O_{13-n}(OH)_n\{(OCH_2)_3CCH_3\}_2]^{1-}$$

$$E = -0.09 \text{ V}, n = 2$$

$$E = -0.32 \text{ V}, n = 4$$

$$E = -0.95 \text{ V}, n = 6$$

The CV of the reduced complex **7** quite unexpectedly exhibits a quasi-reversible one-electron reduction at −1.72 V in addition to the oxidation process discussed above. The product of the reduction is extremely unstable, and no further characterization was possible.

Complexes **6** and **7** may be generated electrochemically from **5c** by successive protonation and reduction steps. Thus, treatment of a solution of **5c** with 2 equiv of HBF_4 produces a brown solution with a quasi-reversible reduction process at −0.85 V. Controlled potential electrolysis of this solution at −0.90 V results in the consumption of 2 faradays mol^{-1} upon complete electrolysis. The electronic spectrum of this species is identical to that of **6**. Addition of a further 2 equiv of HBF_4 to a solution of **6** produces a dark solution whose CV shows an ill-defined cathodic wave at −1.10 V. Controlled potential electrolysis at −1.20 V produces a purple solution upon complete electrolysis with the passage of 2 faradays mol^{-1}. The electronic spectrum of this latter solution is identical to that of **7**. The successive protonation and electrochemical reductions may be summarized as follows:

$$[V^{V}_6O_{13}\{(OCH_2)_3CCH_3\}_2]^{2-} \text{ (3)} \xrightarrow{2H^+/2e^-} [V^{V}_4V^{IV}_2O_{11}(OH)_2\{(OCH_2)_3CCH_3\}_2]^{2-} \text{ (5c)} \xrightarrow{2H^+/2e^-} [V^{V}_2V^{IV}_4O_9(OH)_4\{(OCH_2)_3CCH_3\}_2]^{2-} \text{ (6)} \xrightarrow{2H^+/2e^-} [V^{IV}_6O_7(OH)_6\{(OCH_2)_3CCH_3\}_2]^{2-} \text{ (7)}$$

Attempts to isolate the intermediate products, $[V^{V}_3V^{IV}_5O_{10}(OH)_3\{(OCH_2)_3CCH_3\}_2]^{2-}$ and $[V^{IV}_5V^{V}O_8(OH)_5\{(OCH_2)_3CCH_3\}_2]^{2-}$, proved unsuccessful and invariably resulted in mixtures of **5c** and **6** or **6** and **7**.

EPR Study of $[V^{V}_5V^{IV}O_{13}\{(OCH_2)_3CNO_2\}_2]^{3-}$. The electrochemically generated one-electron species **3b** gave a well-behaved EPR spectrum, which was studied in considerable detail.

The EPR spectra recorded at 4.2, 15, 30, 45, 55, and 83 K (Figure 5A–F) provide a marked change in line shape as the temperature was raised. Individual features, especially the outlying

(37) Pope, M. T.; Papaconstantinou, E.; Varga, G. J., Jr.; Wexell, D. R. *Progress in Coordination Chemistry*; M. Cais, Ed.; Elsevier: New York, 1968, p 322.

(38) Hine, J. *Structural Effects on Equilibria in Organic Chemistry*; J. Wiley and Sons: New York, 1975.

(39) Gordon, A. J.; Ford, R. A. *The Chemists Companion*; J. Wiley and Sons: New York, 1972.

(40) Zuman, P. *Substituent Effects in Organic Polarography*; Plenum Press: New York, 1967.

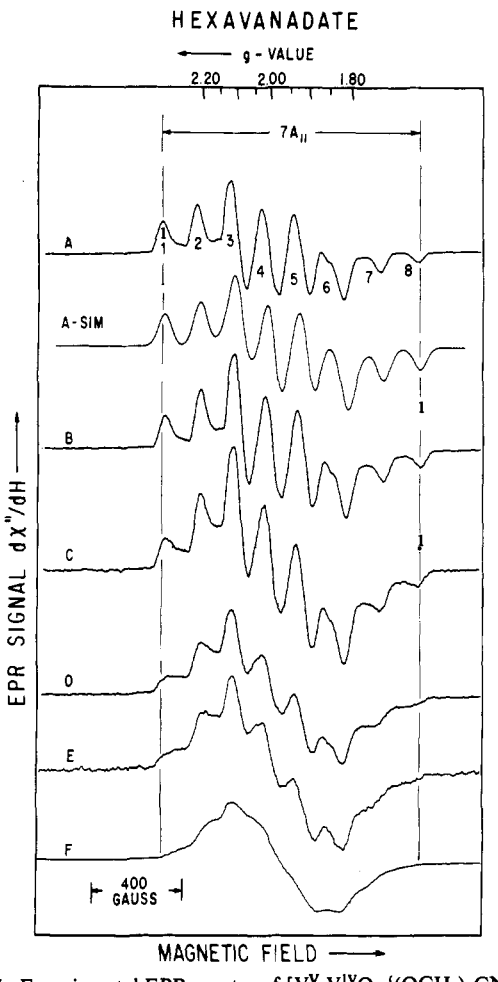

Figure 5. Experimental EPR spectra of $[V^{V}_{5}V^{IV}O_{13}\{(OCH_2)_3CNO_2\}_2]^{3-}$ as recorded at the following temperatures: A, 4.2 K; B, 15 K; C, 30 K; D, 45 K; E, 55 K; F, 83 K. Each spectrum represents four accumulations of 100 s/accumulation. The relative gains for A, B, C, D, E, and F were respectively 1, 5, 15, 15, 24, and 30, and the microwave powers were respectively 4, 25, 70, 70, 70, and 400 μW. The simulated spectrum, A-SIM, was obtained by the use of QPOWA. The relevant parameters for the simulation were as follows: $g_{\parallel} = 1.946$, $A_{\parallel} = 425$ MHz, parallel line width = 85 MHz, $g_{\perp} = 1.956$, $A_{\perp} = 140$ MHz, perpendicular line width = 192 MHz; EPR frequency $\bar{\nu}_0 = 9.124$ GHz, and an intrinsic Gaussian line shape.

ones, became broader. By 83 K, most of the detail observed at lower temperatures had been lost, and the splitting between the outlying features (labeled 1 and 8) diminished as the temperature was raised. At 4.2 and 15 K, the splitting between features 1 and 8 was 1092 G, and at 30, 45, 55, and 83 K this splitting became respectively 1087, 1044, 1014, and 966 G. Features at 83 K from the 5 mM solution were slightly broader than from the 1 mM solution, but at 4.2 K the spectral line shapes from both concentrations were identical. At both 15 and 83 K the integrated intensity of the 5 mM hexavanadium complex was 6-fold larger than that of the 1 mM Cu^{2+} standard; given the experimental uncertainty in spin quantitation, this indicated no marked deviation at either temperature from the expected single unpaired electron per hexavanadium complex. The saturation recovery spin–lattice relaxation times, T_1, as measured at 4.2 K were about 20 ms at the outlying extremes of the EPR spectrum and 10 ms at the center. These relaxation times increased 2-fold in going to 2.1 K. Pulse field-sweep EPR,[21b] a microwave hole-burning technique, enabled us to observe proton spin-flip transitions excited within the EPR line at 2.1 K.

The spectra at 4.2 and 15 K distinctly showed the eight EPR features that would be produced through hyperfine coupling to an electron localized on a *single* $I = {}^{7}/_{2}$ ^{51}V nucleus. If there were significant magnetic interactions between paramagnetic centers, as have been reported for dimeric vanadyl chelates, there would be more lines than the eight expected for one vanadyl nucleus.[41] The distinctive low field "absorption" (1 and 2) and high field "emission" (7 and 8) features are characteristic of frozen solution spectral line shapes for paramagnetic centers that have axial symmetry.[42] The appropriate axial spin Hamiltonian which includes the electron Zeeman interaction and the electron–vanadium nuclear hyperfine interaction is

$$\mathcal{H} = \beta_e(g_{\perp}S_x + g_{\perp}S_y + g_{\parallel}S_z) + h(A_{\perp}S_x + A_{\perp}S_y + A_{\parallel}S_z)$$

where x, y, z is the axis system that diagonalizes the **g** and nuclear hyperfine **A** tensors. The z direction is taken as the parallel direction, while the x and y directions are taken as the perpendicular directions. **A** is expressed in hertz; β_e, h, and **H** are the electron Bohr magneton, Planck's constant, and the applied magnetic field in gauss, respectively. S_i and I_i are the electron and nuclear spin operators.

The outlying $m_I = -{}^{7}/_{2}$ and $+{}^{7}/_{2}$ hyperfine features (i.e., features 1 and 8) of the $I = {}^{7}/_{2}$ ^{51}V nuclear manifold have typically been used to estimate **A** and **g** from frozen solution vanadyl spectra.[43,44] The splitting between the two outermost features in the 4.2 K frozen solution pattern is $7\mathbf{A} = 1092 \pm 20$ G. Thus, $A_{\parallel} = 156 \pm 3$ G, 425 ± 9 MHz, or $(142 \pm 3) \times 10^{-4}$ cm^{-1}. The average resonance field of features 1 and 8 gives $g_{\parallel} = 1.946 + 0.002$ to first order.

At temperatures of 30 K and below, the splitting between each adjacent feature from 1 to 8 remained at approximately $A_{\parallel}$; so the spectral details at 4.2, 15, and 30 K were dominated by the "parallel" part of the frozen solution pattern. The line widths from the resolved parallel features at 4.2 and 15 K were somewhat larger than those shown for monomeric vanadyl complexes by Chasteen[43] and remained so even in a sample prepared at 0.1 mM concentration; the implication is that any broadening is not caused by spin–spin interactions between different hexavanadium clusters. Numerous monomeric vanadyl complexes have shown additional smaller splittings on the order of 60–80 G near the center of their frozen solution spectra, where such features are contributed by magnetic field orientations perpendicular to the unique, short V–O bond axis.[43] Such perpendicular features were not obvious here.

A major goal of the EPR study was to determine the electronic structure of the singly reduced hexavanadium complex in light of X-ray crystallographic results. This meant that we were to characterize the site where the unpaired electrons resided at low temperature, and as the temperature was raised, we were to obtain evidence for motion of the unpaired electron.

A. Localized Site for the Unpaired Spin. At temperatures below 30 K the spectra were frozen solution patterns of a single V(IV) in an axially symmetric environment. The very presence of the additional electron which creates a V(IV) site may cause strains or distortions which at very low temperature lock the electron on that site; slight distortions in bond lengths about a V(IV) site are reported in the X-ray results (vide infra). In the frozen solution spectra of mononuclear vanadyl complexes, the "parallel" features, which account for the details of our spectra, arise from orientations of the magnetic field along the unique, short V–O bond, which determines the "parallel" direction in the spin Hamiltonian.[43] The

(41) Belford, R. L.; Chasteen, N. D.; Tapscott, R. E.; So, H. *J. Am. Chem. Soc.* **1969**, *91*, 4675–4680.

(42) Bruno, G. V.; Harrington, J. K.; Eastman. *J. Phys. Chem.* **1977**, *81*, 1111–1117.

(43) Chasteen, N. D. Vanadyl(IV) EPR Spin Probes: Inorganic and Biochemical Aspects. In *Biological Magnetic Resonance*; Berliner, L. J., Reuben, J., Eds.; Plenum Press: New York, 1981; Vol. 3, Chapter 2.

(44) According to eq 15 of Chasteen (ref 43, p 72), the splitting in Gauss between two hyperfine features with nuclear quantum numbers m_i and m_j in the "parallel" direction should be $[A_{\parallel}(m_i - m_j) + (A_{\perp}{}^2/2\bar{\nu}_0)(m_i{}^2 - m_j{}^2)]/g_{\parallel}\beta_e$, where $\bar{\nu}_0$ is the EPR frequency of 9.126 GHz. Thus the splitting between features 3 and 1, which have $m_i = -{}^{3}/_{2}$ and $m_j = -{}^{7}/_{2}$, will be $(2A_{\parallel} - 5A_{\perp}{}^2/2\bar{\nu}_0)/g_{\parallel}\beta_e$. The splitting between features 8 and 6, which have $m_i = {}^{7}/_{2}$ and $m_j = {}^{3}/_{2}$, will be $(2A_{\parallel} + 5A_{\perp}{}^2/2\bar{\nu}_0)/g_{\parallel}\beta_e$. Since the experimental splitting between features 6 and 8 was 30 G larger than between features 1 and 3, 30 G = $(10A_{\perp}{}^2/\bar{\nu}_0)/g_{\parallel}\beta_e$ and $A_{\perp} = 270$ MHz. However, we discovered during our simulation of Figure 5A-SIM tha an appropriate combination of line widths, g-values, and hyperfine couplings can cause differences comparable to 30 G in splittings between features 1 and 3 vs 6 and 8, even though the value of $A_{\perp}$ was only 140 MHz.

specific values of $A_{\parallel}$ and $g_{\parallel}$ for this site are in the general range found for a number of vanadyl complexes having oxygen ligands,[43] where the unpaired electron is largely in a d_{xy} nonbonding metal orbital.

For comparison to the experimental low-temperature spectrum of Figure 5A, Figure 5A-SIM shows a frozen solution simulation using axial spin Hamiltonian parameters. The major details of the simulated spectrum were obviously sensitive to **A** and **g**. However, it was not obvious either directly from the EPR spectrum or from simulations of it precisely what the values of **A** and **g** ought to be. (See footnote 44 for the estimation of **A** from second-order corrections to hyperfine splittings.) We were led to conclude that the line widths of features in the perpendicular orientations are comparable with **A**. Variation in **g** and **A** did somewhat perturb the intensities of central features 3–6, and **g** = 1.965, a relatively small **A** = 140 MHz, and a large line width in perpendicular directions gave the best overall agreement between simulation and experiment.

B. Evidence for Motion. The EPR spectra clearly showed change in line shape from a localized axial EPR spectrum at 4.2 K to a spectrum at 83 K which exhibited broadening of all features and especially shifting of the outermost features toward the center. Low-temperature dynamic effects as seen with this partially reduced hexavanadate are an unusual phenomenon not observed with monomeric VO^{2+} complexes which "consistently give relatively sharp EPR spectra in both frozen and room temperature solutions".[43] However, similar phenomena setting in above ca. 100 K were observed by EPR from mixed-valence vanadium centers ($V^{IV}V^{V}$ or $V^{IV}V^{V}_2$) contained in heteropolytungstates.[28]

Our work gives evidence for temperature-dependent mobility of the unpaired electron. A motional process, in which an electron hopped from V^{IV} to V^{V} (and so on), would move an unpaired spin between different sites having different magnetic interactions. The magnetic interactions could differ between two different vanadium atoms either because the nuclear m_I spin states of two different atoms are uncorrelated or because the two atoms have a different orientation for the **g** and **A** tensors. Since the short, terminal V–O bond is observed in all complexes here, and since the short V–O bond determines the parallel direction for EPR,[43] the motion which affects our EPR spectra is unlikely to be interconversion of axes on a single site. Rather, it is transfer of an unpaired electron from one vanadium to another. We speculate that the reason for this temperature dependence is coupling of low-energy thermal modes of the complex to electron transfer.

When the rate of hopping becomes comparable with the spectral fequency difference (in rad/s) between interconverting features, individual features will be motionally broadened, and their magnetic field position will tend to an average position.[45] We wanted to estimate a hopping time from the spectral changes. Tumbling of monomeric vanadyl complexes in solution is a motional process in which parallel and perpendicular directions interconvert, and tumbling causes spectral shifts similar to those we see here. As the tumbling rate becomes comparable with $(A_{\parallel} - A_{\perp}) \sim 10^9$ rad/s, the outer features broaden and shift toward each other. Semiempirical formulas have been developed to relate the separation of outlying EPR features to a tumbling correlation time.[42,46] Details of tumbling motion are different from hopping; however, we propose that the relation between tumbling correlation time and separation of outlying features should give at least a semiquantitative estimate for the relation between hopping correlation time and the separation of the same outlying features. At 30, 45, 55, and 83 K the relevant respective correlation times were thus >100, 4.3, 1.8, and 0.7 ns.

Our EPR line widths even at 4.2 K are broad by the standard of most monomeric vanadyl complexes.[43] We considered the possibility that at liquid helium temperatures tunneling, rather than thermally assisted hopping, might cause broadening and rapid spectral diffusion within the EPR line. Our ability at 2.1 K to burn a saturated hole in the EPR line and to observe saturation recovery times in the 10-ms range is evidence against such a tunneling process. The breadth of the EPR line may represent a static, strain-induced difference between sites, or conceivably, the breadth may be due to small unresolved couplings to vanadium neighbors of the V^{IV} site where the electron is localized at liquid helium temperatures. In those heteropolytungstates where two or three adjacent tungsten atoms were replaced by vanadium, superhyperfine structure was directly resolved at ~40 K from vanadium neighbor(s) of the localized V^{IV} site.[28]

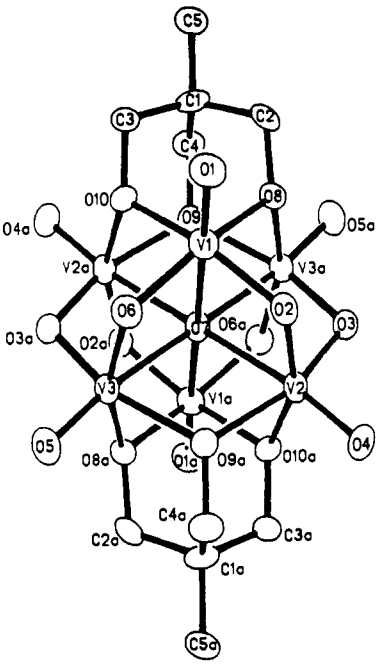

Figure 6. ORTEP view of the structure of $[V_6O_{13}\{(OCH_2)_3CCH_3\}_2]^{2-}$ (**3**), showing the atom-labeling scheme.

Solid-State Structures. X-ray structural analyses of **1–3** and **5–7** revealed that the complexes possess the common hexametalate core $[M_6O_{19}]$ as shown in Figure 6, but perturbed by the presence of the trisalkoxy ligands, by protonation of doubly bridging oxo groups, and/or by reduction of variable numbers of vanadium sites. Selected bond lengths and angles for the oxidized V(V) clusters **1–3** and the protonated V(V) cluster **5** are collected in Table IV, while Table V presents selected metrical parameters for the partially reduced cluster **6** and the fully reduced V(IV) species **7**. Relevant bond lengths and angles for all six structures are compared in Table VI.

The structures of **1–3** are composed of discrete $(n\text{-}C_4H_9)_4N^+$ cations and $[V_6O_{13}\{(OCH_2)_3CR\}_2]^{2-}$ anions and, in the case of **2**, a discrete DMF molecule of crystallization. The structure of the $[V_6O_{13}\{(OCH_2)_3CCH_3\}_2]^{2-}$ anion, shown in Figure 6, is representative of the oxidized hexavanadate complexes. The structure may be viewed in terms of two $[RC(CH_2O)_3]^{3+}$ subunits bound to a $[V_6O_{13}]^{4-}$ core or, alternatively, as the hexametalate core $[V_6O_{19}]^{8-}$ supporting two $[RC(CH_2)_3]^{3-}$ subunits. The trisalkoxy ligands $[RC(CH_2O)_3]^{3-}$ occupy opposite faces of the hexametalate $[V_6]$ octahedron.

The presence of the trisalkoxy ligands serves to deform the regular hexametalate core. Thus, whereas the highly symmetrical hexametalate structures, such as $[Mo_6O_{19}]^{2-}$,[47] $[W_6O_{19}]^{2-}$,[48] and $[Ta_6O_{19}]^{8-}$,[49] each exhibit 12 doubly bridging oxo groups with essentially equivalent M–O distances, the hexavanadate structures $[V_6O_{13}\{(OCH_2)_3CR\}_2]^{2-}$ possess six doubly bridging oxo groups

(45) Carrington, A.; McLachlan, A. D. *Introduction to Magnetic Resonance with Applications to Chemistry and Chemical Physics*; Harper & Row: New York, 1967; Chapter 12.

(46) The correlation time, τ, for tumbling in the case of Brownian rotational diffusion of vanadyl acetylacetonate toluene is $\tau = a(1 - \Delta/7A_{\parallel})^b$ where Δ is the separation (in gauss) between the two outermost peaks, $a = 1.38 \times 10^{-11}$ s/rad, and $b = 1.84$.

(47) Nagano, O.; Sasaki, Y. *Acta Crystallogr.* **1979**, *B35*, 2387.

(48) Fuchs, J.; Freiwald, W.; Hartl, H. *Acta Crystallogr.* **1978**, *B34*, 1764.

(49) See ref 2, p 21.

Table IV. Selected Bond Lengths (Å) and Angles (deg) for $[(C_4H_9)_4N]_2[V_6O_{13}\{(OCH_2)_3CR\}_2]$ (R = NO_2, **1**; CH_2OH, **2**; CH_3, **3**) and for $[V_6O_{11}(OH)_2\{(OCH_2)_3CCH_3\}_2]\cdot 2DMF\cdot(C_2H_5)_2O$ (**5**)

	1	2	3	5
V1–O1	1.599 (2)	1.596 (4)	1.598 (5)	1.593 (4)
V1–O2	1.826 (2)	1.820 (4)	1.802 (6)	1.829 (4)
V1–O6	1.833 (3)	1.833 (4)	1.837 (3)	1.852 (4)
V1–O7	2.239 (1)	2.247 (1)	2.252 (1)	2.219 (2)
V1–O8	2.021 (3)	2.003 (4)	2.107 (7)	1.991 (4)
V1–O10	2.027 (2)	2.032 (3)	2.021 (5)	2.009 (4)
V2–O2	1.809 (3)	1.829 (4)	1.840 (5)	1.812 (4)
V2–O3	1.818 (3)	1.808 (4)	1.820 (6)	1.874 (4)
V2–O4	1.603 (2)	1.598 (4)	1.596 (6)	1.592 (4)
V2–O7	2.253 (1)	2.245 (1)	2.241 (2)	2.249 (1)
V2–O9a	2.028 (3)	2.032 (4)	2.021 (7)	1.998 (4)
V2–O10a	2.034 (2)	2.007 (3)	2.010 (5)	1.993 (4)
V3–O5	1.607 (3)	1.598 (4)	1.603 (7)	1.594 (4)
V3–O6	1.809 (2)	1.819 (3)	1.821 (5)	1.788 (4)
V3–O7	2.239 (1)	2.232 (1)	2.233 (2)	2.256 (2)
V3–O3a	1.817 (2)	1.834 (3)	1.835 (5)	1.884 (4)
V3–O8a	2.027 (3)	2.019 (3)	2.023 (5)	2.029 (4)
V3–O9a	2.033 (2)	2.024 (4)	2.018 (7)	1.994 (4)
O1–V1–O7	170.8 (1)	172.6 (1)	172.3 (2)	173.0 (2)
O2–V1–O10	158.1 (1)	157.7 (2)	157.5 (2)	158.4 (2)
O6–V1–O8	158.0 (1)	157.5 (2)	157.4 (2)	158.4 (2)
O2–V2–O10a	157.6 (1)	157.8 (2)	157.4 (3)	157.6 (2)
O3–V2–O9a	157.3 (1)	158.4 (2)	158.7 (2)	158.8 (2)
O4–V2–O7	171.7 (1)	171.3 (1)	171.7 (2)	173.6 (2)
O5–V3–O7	171.7 (1)	171.9 (1)	172.2 (3)	172.8 (2)
O6–V3–O8a	158.4 (1)	158.3 (2)	158.7 (3)	157.6 (2)
O3a–V3–O9a	157.8 (1)	158.6 (2)	158.7 (3)	158.1 (2)
V1–O2–V2	112.5 (1)	112.6 (2)	112.8 (2)	112.8 (2)
V2–O3–V3a	113.1 (1)	112.2 (2)	111.2 (4)	111.3 (2)
V1–O6–V3	111.7 (2)	112.1 (2)	112.3 (3)	112.8 (2)

and six doubly bridging alkoxy groups with average V–O distances of 1.823 (4) and 2.022 (4) Å, respectively. Aside from the structures of this study, the hexavanadate core has been reported in a single instance, that of the organometal oxide $[(C_5Me_5)Rh]_4[V_6O_{19}]$.[50] In this latter case, the 12 triply bridging oxo groups of the $[V_2RhO]$ class exhibit nearly equivalent V–O distances of 1.916 (4) Å. Thus, although the structural cores of **1–3** are grossly similar to that of $[(C_5Me_5)Rh]_4[V_6O_{19}]$, the former structures are significantly distorted from the more or less regular $[V_6O_{19}]^{8-}$ "superoctahedral" core of the Rh analogue.

The structural consequences of protonation of the hexavanadate core are revealed in the structure of $[V_6O_{11}(OH)_2\{(OCH_2)_3CCH_3\}_2]$ (**5**). As shown by the comparison of structural parameters of **5** with those of **1–3**, the only pronounced effect of protonation is an expansion of V2–O3 and V3–O3a distances to 1.874 (4) and 1.884 (4) Å, respectively, from the average value of 1.823 (4) Å observed for unprotonated, doubly bridging oxo groups. The locations of protonation as O3 and O3a were revealed clearly in the difference Fourier maps for the structure of **5**, and this conclusion is also supported by bond length–bond number calculations, using the empirical parameters developed by Brown and Wu.[51] Calculations based on all the oxygen atoms of **5** give a bond number of 2.00 valence units for the central oxygen O7 and values averaging 1.98 valence units for O2, O6, and O7–O10. In contrast, in the absence of protonation, the valence sum for O3 is 1.57 valence units. Allowing for the presence of H3, the sum is 1.97, confirming the observations of the direct crystallographic analysis.

The most extreme structural changes are observed in the fully reduced or six-electron, six hydroxy group cluster $[V_6O_7(OH)_6\{(OCH_2)_3CCH_3\}_2]^{2-}$, whose structure is shown in Figure 7. Complex **7** retains the hexavanadate core, but with all six doubly bridging oxo groups protonated and all six vanadium centers in the V(IV) oxidation sate. These changes are most obviously reflected in the bond lengths of the vanadium–bridging hydroxy group interactions. As illustrated by Table VI, the average V–

Table V. Selected Bond Lengths (Å) and Angles (deg) for $[(C_4H_9)_4N]_2[V_6O_9(OH)_4\{(OCH_2)_3CCH_3\}_2]$ (**6**) and $[(C_4H_9)_4N]_2[V_6O_7(OH)_6\{(OCH_2)_3CCH_3\}_2]\cdot 2CH_2Cl_2\cdot 0.5C_6H_5NNC_6H_5$ (**7**)

	6[a]	7[a]	7[b]	
V1–O1	1.608 (3)	1.610 (3)	1.601 (3)	V4–O11
V1–O2	1.940 (4)	2.004 (4)	1.986 (4)	V4–O12
V1–O6	1.926 (4)	2.000 (4)	2.000 (3)	V4–O16
V1–O7	2.304 (1)	2.322 (1)	2.324 (1)	V4–O17
V1–O8	2.008 (4)	1.995 (3)	2.006 (3)	V4–O18
V1–O10	2.006 (3)	2.015 (3)	2.001 (3)	V4–O10
V2–O2	1.952 (3)	2.005 (4)	1.990 (3)	V5–O12
V2–O3	1.869 (4)	1.970 (4)	1.992 (3)	N5–O13
V2–O4	1.596 (4)	1.604 (4)	1.612 (4)	V5–O14
V2–O7	2.284 (1)	2.304 (1)	2.284 (1)	V5–O17
V2–O9a	2.038 (4)	1.997 (3)	2.007 (3)	V5–O19a
V2–O10a	2.000 (3)	2.008 (3)	2.002 (3)	V5–O20a
V3–O5	1.609 (4)	1.594 (4)	1.607 (3)	V6–O15
V3–O6	1.936 (3)	2.019 (4)	2.002 (3)	V6–O16
V3–O7	2.273 (1)	2.310 (1)	2.314 (1)	V6–O17
V3–O3a	1.975 (3)	1.973 (5)	1.991 (4)	V6–O13a
V3–O8a	2.016 (3)	2.004 (3)	1.996 (3)	V6–O18a
V3–O9a	1.990 (4)	2.014 (3)	2.007 (3)	V6–O19a
O2–H2	1.00 (4)	0.68 (5)	0.78 (4)	O12–H12
O3–H3	–	0.76 (5)	0.73 (6)	O13–H13
O6–H6	1.01 (3)	0.70 (5)	0.73 (7)	O16–H16
O1–V1–O7	177.4 (1)	178.5 (1)	178.9 (1)	O11–V4–O17
O2–V1–O10	158.9 (1)	160.2 (1)	159.5 (1)	O12–V4–O20
O6–V1–O8	158.8 (1)	160.4 (1)	159.5 (1)	O16–V4–O18
O2–V2–O10a	159.3 (2)	161.2 (1)	161.3 (1)	O12–V5–O20a
O3–V2–O9a	160.4 (2)	160.0 (2)	161.7 (1)	O13–V5–O19a
O4–V2–O7	174.8 (2)	179.3 (1)	179.5 (1)	O14–V5–O17
O5–V3–O7	178.3 (1)	177.8 (1)	178.4 (1)	O15–V6–O17
O6–V3–O8a	160.3 (2)	160.5 (1)	160.2 (1)	O16–V6–O18a
O3a–V3–O9a	159.6 (2)	159.2 (2)	160.4 (1)	O13a–V6–O19a
V1–O2–V2	110.7 (1)	110.2 (2)	109.6 (2)	V4–O12–V5
V2–O3–V3a	110.3 (1)	112.0 (2)	108.9 (2)	V5–O13–V6a
V1–O6–V3	111.7 (2)	109.6 (2)	110.4 (2)	V4–O16–V6
V1–O2–H2	105.6 (52)	105.9 (42)	105.6 (35)	V4–O12–H12
V2–O2–H2	109.8 (54)	107.2 (41)	118.8 (31)	V5–O12–H12
V2–O3–H3	–	116.6 (54)	107.8 (49)	V5–O13–H13
V3a–O3–H3	–	113.9 (53)	108.9 (57)	V6a–O13–H13
V1–O6–H6	106.4 (48)	106.8 (38)	107.5 (42)	V4–O16–H16
V3–O6–H6	112.2 (52)	111.0 (34)	99.5 (48)	V6–O16–H16

[a] Bond lengths and angles for **6** and the first column of **7** are identified by the left-hand column. [b] Bond lengths and angles for the second column of **7** are identified by the right-hand column.

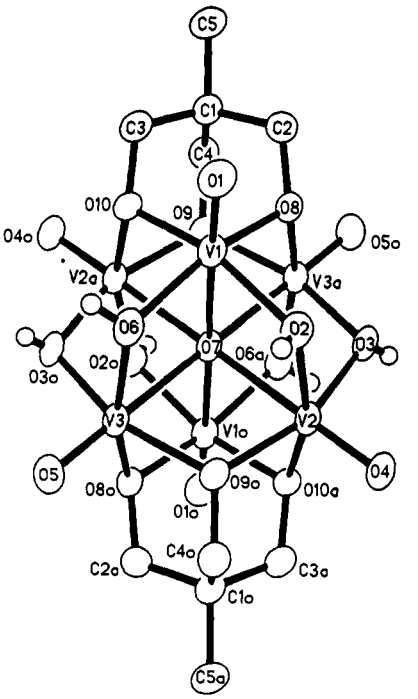

Figure 7. A view of the structure of $[V_6O_7(OH)_6\{(OCH_2)_3CCH_3\}_2]^{2-}$ (**7**).

(50) Chae, H. K.; Klemperer, W. G.; Day, V. W. *Inorg. Chem.* **1989**, *28*, 1424. Hayaski, Y.; Ozawa, Y.; Isobe, K. *Chem. Lett.* **1989**, 425.
(51) Brown, I. D.; Wu, K. K. *Acta Crystallogr.* **1976**, *B32*, 1957.

Table VI. Comparison of Selected Bond Lengths (Å) and Angles (deg) for the Fully Oxidized Clusters $[V_6O_{13}\{(OCH_2)_3CR\}_2]^{2-}$ (**1–3**) and $[V_6O_{11}(OH)_2\{(OCH_2)_3CCH_3\}_2]$ (**5**), the Mixed-Valence Cluster $[V_6O_9(OH)_4\{(OCH_2)_3CCH_3\}_2]^{2-}$ (**6**), and the Fully Reduced V(IV) Cluster $[V_6O_7(OH)_6\{(OCH_2)_3CCH_3\}_2]^{2-}$ (**7**)

bond or angle[a]	average value[b] for 1–3	average value for 5	Δ[c]	average value for 6	Δ′[d]	Δ″[e]	average value for 7	Δ‴[f]	Δ+[g]	Δ++[h]
$V-O_t$	1.600 (4,4,7,9)	1.593 (4,1,1,3)	–	1.604 (4,5,8,3)	+0.004	+0.011	1.605 (4,7,11,16)	+0.005	+0.012	+0.001
$V-O_b(H)$	1.823 (4,21,17,18)	1.879 (4,5,5,2)	–	1.946 (4,20,29,5)	+0.123	+0.067	1.994 (4,24,25,2)	+0.171	+0.115	+0.048
		1.820 (4,22,42,4)	–	1.869 (4,–,–,1)	+0.046	+0.049			+0.174	+0.125
$V-O_{alkoxy}$	2.022 (4,19,12,18)	1.994 (4,3,4,4)	–	2.004 (4,12,14,5)	–0.018	+0.010	2.004 (4,9,11,12)	–0.018	+0.010	0.000
		2.019 (4,10,10,2)	–	2.038 (4,–,–,1)	+0.016	+0.019			–0.015	–0.034
$V-O_c$	2.242 (1,10,11,9)	2.219 (2,–,–,1)	–0.013	2.287 (1,14,17,3)	+0.045	–	2.308 (1,16,24,6)	+0.066	+0.089	+0.021
		2.253 (2,4,4,2)	+0.011						+0.055	
$V-O_b-V$	112.3 (2,11,8,9)	112.1 (2,8,7,3)	–0.002	110.9 (1,6,8,3)	–1.4	–	110.1 (2,12,19,6)	–2.2	–2.0	–0.8

[a] Abbreviations used are as follows: $O_t \equiv$ terminal oxo group; $O_b(H) \equiv$ doubly bridging oxo or hydroxy group; $O_{alkoxy} \equiv$ oxygen donor of the trialkoxy ligand; $O_c \equiv$ central oxo group. [b] The first number in parentheses following an average value of a bond length or bond angle is the root-mean-square estimated standard deviation of an individual datum. The second and third numbers, when given, are the average and maximum deviations from the averaged value, respectively. The fourth number represents the number of individual measurements that are included in the average value. [c] The differences between the average values for **5** and those of **1–3**. [d] The differences between the average values for **6** and those of **1–3**. [e] The differences between the average values for **6** and those for **5**. [f] The differences between the average values for **7** and those of **1–3**. [g] The differences between the average values for **7** and those for **5**. [h] The differences between the average values for **7** and those for **6**.

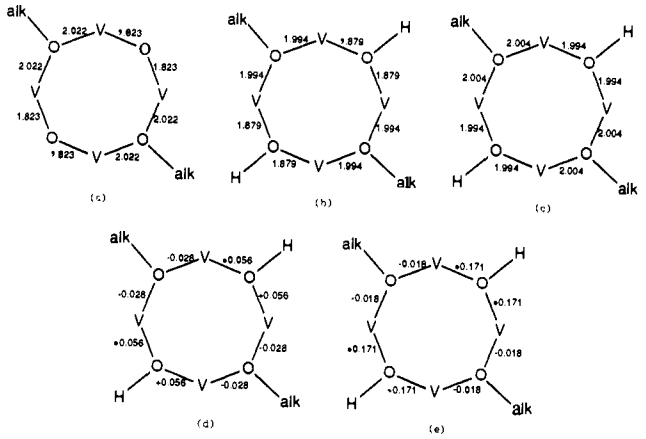

Figure 8. Schematic representations of (a) average V–O distances in the $V_4O_2(OR)_2$ rings of structures **1–3**, (b) V–O distances in the $V_4(OR)_2(OH)_2$ ring of **5**, and (c) V–O distances in the $V_4(OR)_2(OH)_2$ ring of **7** and of the differences in V–O distances in comparing (d) the averages of **1–3** with **5** and (e) the averages of **1–3** with **7**.

O(H) distance for **7** is 1.994 (4) Å, an expansion of +0.171 Å compared to the average vanadium–bridging oxo group distance of 1.823 (4) Å for **1–3**. Since the structural parameters for protonation of doubly bridged oxo groups in the absence of reduction are known from the structure of **5**, the structural consequences of reduction relative to protonation may be assessed. While protonation alone results in an increase of the protonated V–O(bridge) distances by an average of +0.056 Å, protonation coupled to reduction results in a further bond lengthening of +0.115 Å, to give an average increase of +0.171 Å in the structure of **7**. We conclude that reduction alone would be manifest by a bond lengthening of the V–O(bridge) distance of twice the order of magnitude of that produced by protonation alone.

These results are further illustrated diagrammatically in Figure 8. The results tabulated in Table VI show that, in addition to the expected bond lengthenings consequent to reduction and/or protonation, there are a number of small bond contractions in structures **5** and **7** compared to **1–3**. The systematic nature of these bond variations is evident from Figure 10, which shows the bond length alternations for the eight-membered rings V_4O_4 of **1**, and those of **5** and **7** which contain bridging hydroxy groups. Also provided in the figure are the bond length differences in the rings for the V–O bonds of **1** and **5** and **1** and **7**. The result is a pattern of trans bond length alternations similar to those previously reported for $[H_3V_{10}O_{28}]^{3-}$,[7] $[(C_5H_5)TiMo_5O_{18}]^{3-}$,[52] $[(C_5Me_5)Rh][Nb_2W_4O_{19}]^{2-}$,[13h] $[Mn(CO)_3][Nb_2W_4O_{19}]^{3-}$,[13g] $[(C_5H_5)Ti][Mo_5O_{18}MoO_2Cl]^{2-}$,[53] and $[Mn(Nb_6O_{19})_2]^{12-}$.[13e] In the present case, protonation of O3 in **5** removes electron density from the oxygen and weakens the V–O3 bond, resulting in lengthening. Concomitantly, the trans V–O bonds are strengthened and hence shortened. In the case of complex **7**, the effects of protonation are combined with those of reduction of the vanadium sites, which tends to lengthen all V–O bonds. Hence, the cumulative lengthening effect on the V–O(H) bond distances is apparent, while the trans shortening is diminished by the counterpoising influence of the increase in covalent radius of V(IV) relative to V(V).

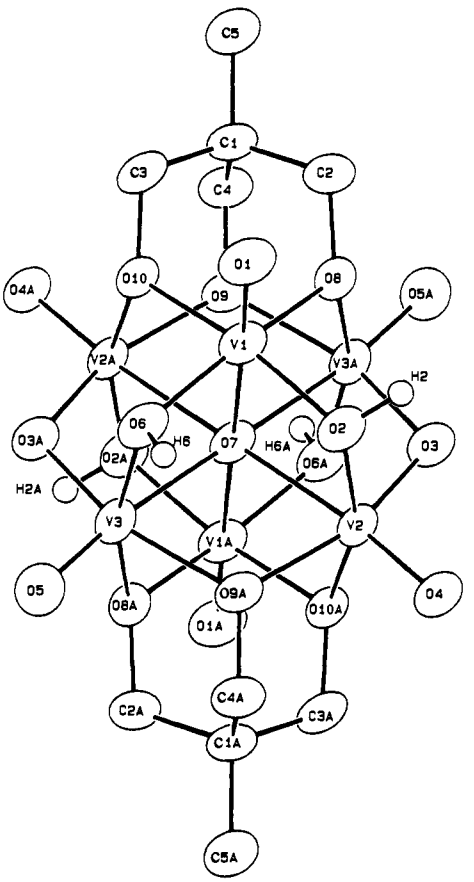

Figure 9. A view of the structure of $[V_6O_9(OH)_4\{(OCH_2)_3CCH_3\}_2]^{2-}$ (**6**).

The bond distances observed for the V–O bonds of **7** are also consistent with valence sum calculations shown in Table VII. Bond length–bond strength correlations of the form $s = (R/R_1)^{-N}$,

(52) Che, T. M.; Day, V. W.; Francesconi, L. C.; Fredrich, M. F.; Klemperer, W. G.; Shum, W. *Inorg. Chem.* **1985**, *24*, 4055.

(53) Day, V. W.; Fredrich, M. F.; Thompson, M. R.; Klemperer, W. G.; Liu, R.-S.; Shum, W. *J. Am. Chem. Soc.* **1981**, *103*, 3597.

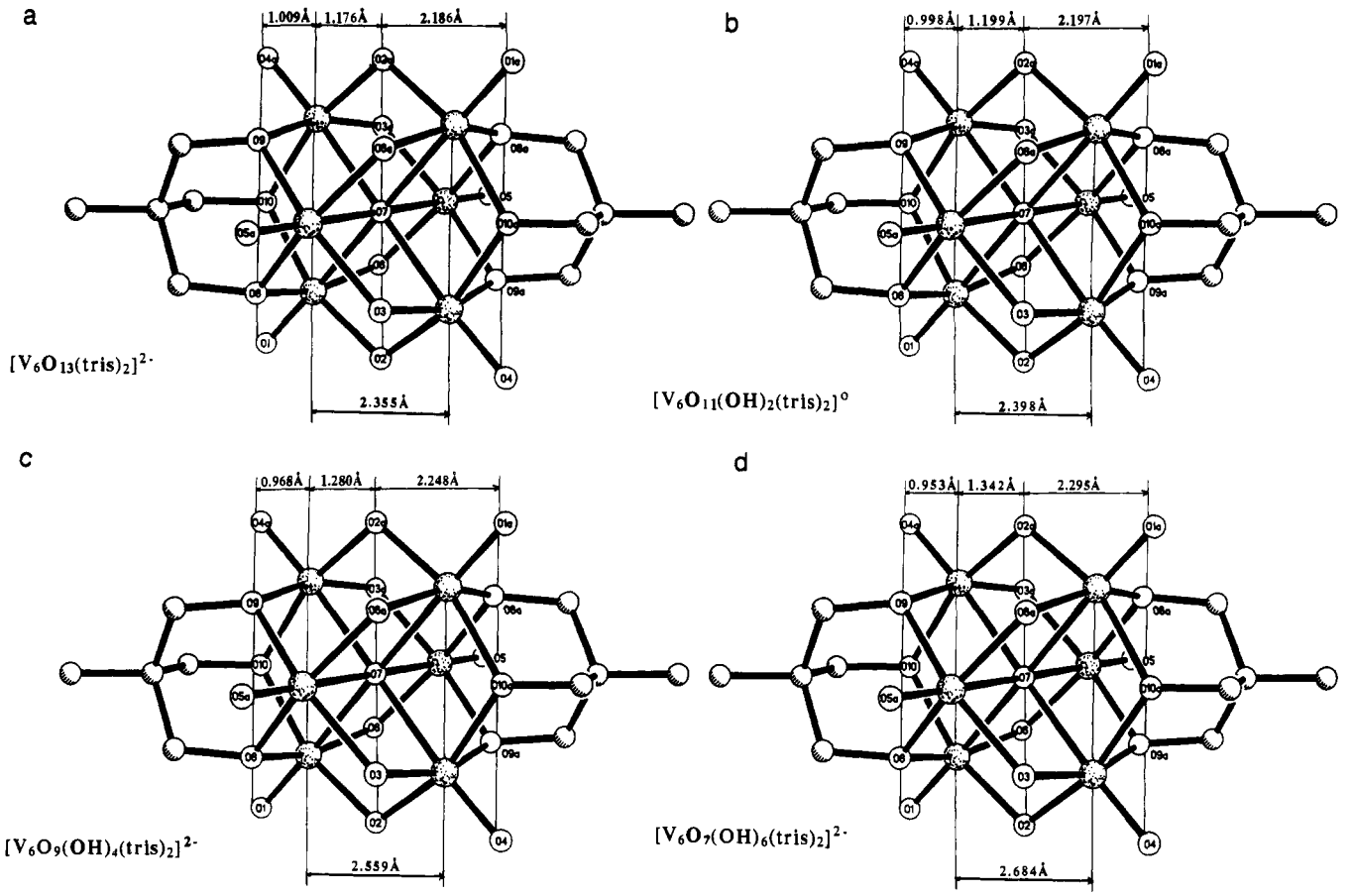

Figure 10. Distances between approximately planar layers of oxygen atoms and layers of vanadium sites for (a) $[V_6O_{13}\{(OCH_2)_3CCH_3\}_2]^{2-}$, (b) $[V_6O_{11}(OH)_2\{(OCH_2)_3CCH_3\}_2]$, (c) $[V_6O_9(OH)_4\{(OCH_2)_3CCH_3\}_2]^{2-}$, and (d) $[V_6O_7(OH)_6\{(OCH_2)_3CCH_3\}_2]^{2-}$.

Table VII. Bond Number Calculations for the Vanadium Centers of the Structures of This Study

complex	average $\sum s_i$, valence units	complex	average $\sum s_i$, valence units
1	5.00[a]	**5**	5.01[a]
2	4.99[a]	**6**	4.36[b]
3	5.02[a]	**7**	4.05[c]

[a] Bond valence sums for the V(V) centers are given by $\sum_i d(V-O_i)/1.791)^{-5.1}$. [b] The distinction between V(V)/V(IV) centers is based on the averaged summation $\sum_i d(V-O_i)/1.78)^{-5.15}$. [c] Bond valence sums for the V(IV) centers are given by $\sum_i d(V-O_i)/1.77)^{-5.2}$.

where s is Pauling's bond strength in valence units, R is the metal–oxygen bond length, and R_1 and N are empirical parameters, have been derived by several authors[51,54] and are used in deriving the valence sums of Table VII. While structures **1–3** and **5** yield valence sums of approximately 5.0, structure **7** clearly conforms to the valence for a cluster with exclusively V(IV) d^1 centers. In contrast, the structure of $[V_6O_9(OH)_4\{(OCH_2)_3CCH_3\}_2]^{2-}$ (**6**) is clearly a mixed-valence species. The calculations indicate an average vanadium valence of 4.36 for **6**, which is consistent with the $V^V_2V^{IV}_4$ formalism.

The structure of the complex anion of **6** is shown in Figure 9. The protonation sites are clearly established by X-ray crystallography as O2 and O6. This conclusion is reinforced by valence sum calculations which yield sums of 1.31 and 1.36 valence units for O2 and O6 in the absence of the hydrogen atoms and sums of 1.96 and 1.99 valence units with protonation. The average V–O(H) bond distance in **6** is 1.939 (4) Å, which may be compared to a value of 1.994 (4) Å in the fully reduced species **7**. This observation is suggestive of a degree of charge delocalization within the cluster. On the other hand, the nonsymmetric bridging character of O3, V2–O3 at 1.869 (4) Å and V3–O3a at 1.975 (3) Å, would seem to suggest that V3 is largely +IV in character, while V2 is in the +V oxidation state. Assuming this limiting-case formalism of $V3^{IV}$ and $V2^{V}$, valence sum calculations provide values of 4.15 and 4.57 valence units for V3 and V2, respectively. While these numbers do not have a precise significance, they do support partial charge delocalization in cluster **6** with some degree of charge asymmetry affecting the bonding to the unique doubly bridging oxo groups.

The structural effects of reduction and/or protonation can also be demonstrated by comparing the spacing between approximately planar layers of negatively charged and close-packed oxygen atoms separated by layers of cationic vanadium centers[7] in the oxidized clusters **1–3**, the protonated species **5**, the mixed-valence polyanion **6**, and the fully reduced six proton cluster **7**, as shown in Figure 10. In all cases, the plane containing the central six-coordinate oxygen atom and the six doubly bridging oxo and/or hydroxy groups defines the reference plane from which the spacings to the other parallel layers (to within 1.2°) have been calculated. There are two types of planes above and below the reference plane: two sets of three terminal oxo groups and three bridging alkoxy oxygen donors and two sets of three vanadium atoms. Figure 10a illustrates the average interplanar spacings for the fully oxidized structures **1–3**. The outermost layers of oxygen atoms are displaced 2.186 Å from the reference plane, while the vanadium layers are situated 1.176 Å from this plane. As anticipated, the vanadium layer is considerably displaced toward the outermost layer of oxygen atoms, away from the reference plane: 1.009 Å to the outermost oxygen layer vs. 1.176 Å to the reference plane. This difference reflects the usual displacement of the metal centers in polyanions from the center of the MO_6 octahedron in the direction of the terminal oxo group. The consequences of protonation of the hexavanadate core in **5** are illustrated in Figure 10b. Protonation of two bridging oxo groups results in an overall expansion of the cluster volume. Closer inspection reveals that the predominant effects reside in the location of the vanadium

(54) Brown, I. D.; Shannon, R. D. *Acta Crystallogr.* **1973**, *A29*, 266.

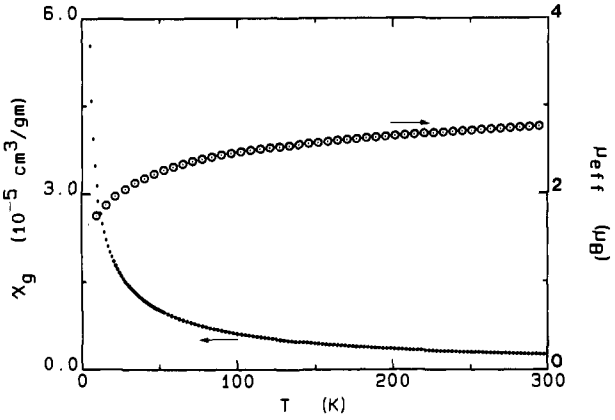

Figure 11. Plot of the susceptibility (χ_g) and the effective moment (μ_{eff}) per molecule for solid **5c**.

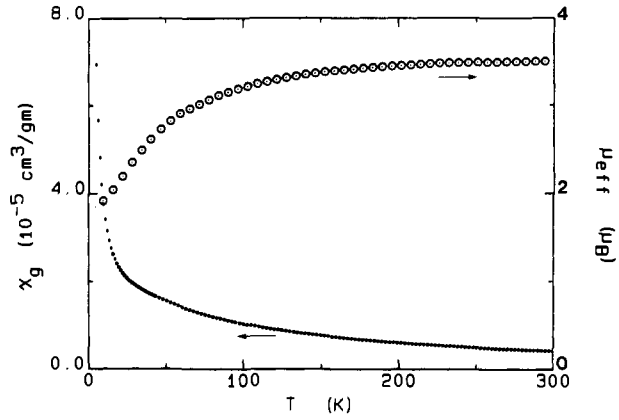

Figure 12. Plot of the susceptibility (χ_g) and the effective moment (μ_{eff}) per molecule for solid **6**.

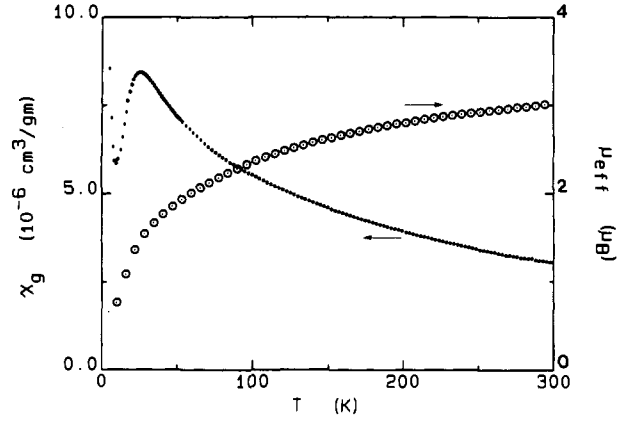

Figure 13. Plot of the susceptibility (χ_g) and the effective moment (μ_{eff}) per molecule for solid **7**.

planes relative to the oxygen layers. Formation of two O–H bonds removes charge from the central layer of oxygens and weakens the bonds between these oxygens and the vanadium layers. Consequently, the vanadium layers move away from the reference plane by 0.023 Å and move 0.011 Å closer to the outermost layer of negatively charged oxygen atoms.

Such effects would be expected to be more pronounced upon coupled protonation and reduction of the core, as a result of the larger covalent radius of V(IV) relative to V(V). The structure of $[V_6O_9(OH)_4\{(OCH_2)_3CCH_3\}_2]^{2-}$ shown in Figure 10c illustrates this point. Protonation of four oxygen atoms of the reference plane, combined with reduction of four vanadium sites, has increased the displacement of the vanadium planes from the reference plane to 1.280 Å, an increase of 0.104 Å relative to the fully oxidized structural types. Since protonation removes charge from the central plane, displacement of the vanadium planes toward the outermost negatively charged oxygen planes is anticipated, and a decrease of the distance between these planes of 0.03 Å compared to that of structure **5** and of 0.054 Å compared to **1** is observed.

The fully reduced, six-proton structure $[V_6O_7(OH)_6\{(OCH_2)_3CCH_3\}_2]^{2-}$ (**7**), shown in Figure 10d, exhibit the most pronounced effects. All the oxygen atoms of the central plane have been protonated, resulting in an expanded distance of 1.342 Å from this plane to the vanadium planes. A monotonic increase in the reference plane to vanadium plane distances is thus observed upon progressing from the oxidized structural core (**1**, **2**, and **3**), to the protonated oxidized cluster (**5**), to the four-electron, four-proton cluster (**6**), and to the fully reduced, six-electron, six-proton polyanion (**7**): 1.176, 1.199, 1.280, and 1.342 Å, respectively. The concomitant decrease in the distance from the outermost oxygen layer to the vanadium plane also progresses smoothly: 1.009 Å for the oxidized clusters, 0.998 Å for **5**, 0.968 Å for **6**, and 0.953 Å for **7**.

The structural changes concomitant to protonation and reduction of the hexavanadate core are also evident in an overall expansion of the core volume as reflected in an increase in the distances between the outermost planes of oxygen atoms in the various structures. While the oxidized core shown in Figure 10a exhibits a distance of 4.37 Å between the outermost oxygen layers, the protonated cluster **5** shows only a marginal expansion to 4.39 Å. The effects of coupled protonation/reduction are more dramatic, as illustrated by distances of 4.50 and 4.59 Å for the mixed-valence cluster (**6**) and for the fully reduced species (**7**), respectively.

Magnetic Behavior. Figures 11–13 show plots of the magnetic susceptibilities (χ_g) and effective moments (μ_{eff}) per molecule[55] for $[(n\text{-}C_4H_9)_4N]_2[V^V_4V^{IV}_2O_{11}(OH)_2\{(OCH_2)_3CCH_3\}_2]$ (**5c**), $[(n\text{-}C_4H_9)_4N]_2[V^V_2V^{IV}_4O_9(OH)_4\{(OCH_2)_3CCH_3\}_2]$ (**6**), and $[(n\text{-}C_4H_9)_4N]_2[V^{IV}_6O_7(OH)_6\{(OCH_2)_3CCH_3\}_2]\cdot 2CH_2Cl_2\cdot 0.5C_6H_5NNC_6H_5$ (**7**). Variable-temperature solid-state magnetic suscpetibility studies were performed on powdered samples of **5c**, **6**, and **7** in the range 4.2–300 K. The effective magnetic moment of **5c** at 300 K is 2.60 μ_B/molecule, which may be compared to a theoretical spin-only moment in the absence of coupling of 2.45 μ_B/molecule. However, the effective magnetic moment of **5c** varies gradually from the value of 2.60 μ_B at 300 K (1.84 μ_B per V(IV) center) to 1.70 μ_B/molecule at 4.2 K (1.20 μ_B per V(IV) center). The data approach Curie–Weiss behavior, $\chi_M = C/(T-\Theta)$, with a Curie temperature Θ of −22.6 K. The magnetic interactions responsible for the deviation of the data from the Curie law $\chi_M = C/T$ are antiferromagnetic, with an upper limit of −1.70 cm^{-1} for J.[56]

Complex **6**, likewise, exhibits approximate Curie–Weiss behavior. The effective magnetic moment (μ_{eff}) per molecule at 300 K is 3.48 μ_B (1.74 μ_B per V(IV) site) and gradually decreases to a value of 1.90 μ_B/molecule (0.95 μ_B per V(IV) site) at 4.2 K. The Curie temperature Θ of −54 K is consistent with antiferromagnetic interactions between the four V(IV) d^1 sites of **6**. The magnetic behavior of **6** lies in the complicated intermediate region for vanadium clusters, where the formal number of V(IV) centers is larger than half of the whole number of V atoms. In these cases, both trapped and delocalized V(IV) centers may occur,[12g] and the valence sum calculations on **6** suggest some degree of localization.

The effective magnetic moment per molecule for **7** is 3.05 μ_B at 300 K, corresponding to 1.25 μ_B per V(IV) center. The moment decreases with temperature to a value of 0.70 μ_B/molecule at 4.2 K (0.29 μ_B per V(IV) site), with a Néel temperature of 26 K, consistent with strong antiferromagnetic coupling between V(IV) sites.

(55) Carlin, R. L. *Magnetochemistry*; Springer-Verlag: Berlin, 1986.

(56) Chen, Q.; Goshorn, D.; Haushalter, R. C.; Zubieta, J. Manuscript in preparation.

(57) Müller, A.; Döring, J.; Khan, M. I.; Wittenben, V. *Angew. Chem., Int. Ed. Engl.* **1991**, *30*, 210.

(58) Müller, A.; Döring, J. *Z. Anorg. Allg. Chem.* **1991**, *595*, 251.

Table VIII. Effective Magnetic Moments of Selected Vanadium Oxygen Clusters with Varying Numbers of V(IV) d^1 Sites

anion	no. of V(IV) centers	μ_{eff}/μ_B per V(IV)[a]	V(IV)···V(IV)[b]	ref
$[V_{14}AsO_{40}]^{7-}$	2	1.77	8.72	57
$[V_{12}As_8O_{40}(HCO)_2]^{3-}$	6	1.75	5.25	12g
$[V_{12}As_8O_{40}(HCO)_2]^{5-}$	8	1.39	c	12g
$[V_{14}As_8O_{42}(SO_3)]^{6-}$	14	1.20	2.81-3.06	58
$[V_6O_{11}(OH)_2\{(OCH_2)_3CCH_3\}_2]^{2-}$	2	1.84	-	this work
$[V_6O_9(OH)_4\{(OCH_2)_3CCH_3\}_2]^{2-}$	4	1.74	3.20-4.60	this work
$[V_6O_7(OH)_6\{(OCH_2)_3CCH_3\}_2]^{2-}$	6	1.25	3.25-4.60	this work

[a] Room temperature. [b] Distances in Å. [c] Complicated intermediate region where the number of formal V(IV) sites is greater than half the total number of V centers.

The magnetic behavior of **5c**, **6**, and **7** is qualitatively similar to that reported for other vanadium-oxygen clusters with varying numbers of V(IV) d^1 centers (Table VIII). In species with a small number of spins, V(IV) d^1 sites, the spins may be trapped and remain as far apart as possible, resulting in nearly spin-only values for μ_{eff} per V(IV). Spin-spin coupling increases with an increasing number of V(IV) centers, which necessarily results in close contacts. A more detailed analysis of the magnetic properties of these and related hexavanadium and decavanadium clusters is being developed.[56]

Conclusions

1. The hexavanadate core $\{V_6O_{19}\}$ is stabilized in the presence of alkoxy ligands. The replacement of bridging oxo groups by bridging alkoxy groups serves to reduce the cluster charge and to stabilize the hexametalate core for vanadium.

2. In the solid state and in solution, the protonation sites of both oxidized and reduced hexavanadate cores have been identified as the doubly bridging oxo groups, establishing these as more nucleophilic/basic than the terminal oxo groups.

3. The hexavanadate cluster readily undergoes coupled reduction/protonation to give the mixed-valence species $[V_6O_9(OH)_4\{(OCH_2)_3CCH_3\}_2]^{2-}$ and the V(IV) cluster $[V_6O_7(OH)_6\{(OCH_2)_3CCH_3\}_2]^{2-}$.

4. Reduction and protonation can be decoupled. Thus, electrochemical reduction of $[V_6O_{13}\{(OCH_2)_3CCH_3\}_2]^{2-}$ (**3**) gives the mixed-valence species $[V^V_5V^{IV}O_{13}\{(OCH_2)_3CCH_3\}_2]^{3-}$, while protonation of **3** yields the neutral polymetalate $[V_6O_{11}(OH)_2\{(OCH_2)_3CCH_3\}_2]$.

Acknowledgment. J.Z. thanks the National Science Foundation for support of this work (CHE8815299 and CHE9119910). Acknowledgment is also made to the donors of the Petroleum Research Fund, administered by the American Chemical Society, for partial support of this research. This work was also supported by NSF Grant BBS 8711617 (C.P.S.) and NIH Grant GM-35103 (C.P.S.). EPR analysis software was furnished by the Illinois ESR Research Center, NIH Division of Research Resources Grant No. RR01811.

Supplementary Material Available: Tables of experimental details and crystal parameters for the structures of **1-3** and **5-7** and tables of atomic positional parameters, bond lengths and angles, anisotropic temperature factors, and calculated hydrogen atom positions for the structures (60 pages); observed and calculated structure factors (135 pages). Ordering information is given on any current masthead page.

Organic Template-Directed Inorganic Crystallization: Oriented Nucleation of $BaSO_4$ under Compressed Langmuir Monolayers

Brigid R. Heywood* and Stephen Mann

Contribution from the School of Chemistry, University of Bath Claverton Down, Bath BA2 7AY, United Kingdom. *Received October 21, 1991. Revised Manuscript Received February 3, 1992*

Abstract: Langmuir monolayers of *n*-eicosyl sulfate were shown to influence the nucleation of $BaSO_4$ grown from supersaturated solutions ($S = 30$) at room temperature (293 K). Thin, elongated single crystalline plates were nucleated with the (100) face parallel to the plane of the monolayer. Partial matching of cation-cation distances with the interheadgroup spacings and stereochemical complementarity between the anionic motif and sulfate headgroups are potential factors responsible for oriented nucleation. The oriented crystals exhibited an unusual texture of coherently intergrown rhombic subunits which was attributable to monolayer-induced growth along specific lattice directions parallel to the monolayer/solution interface. By contrast, barium sulfate crystals nucleated under compressed eicosanoic acid monolayers were oriented along the [010] direction. These crystals were irregular in morphology, suggesting a kinetic rather than a structural influence of the organic template on nucleation at the monolayer/solution interface.

Introduction

Crystal formation involves two major steps: nucleation and growth. Nucleation is favored when relatively long-lived clusters are formed through the aggregation of ions and/or molecular species into stable structural configurations. Growth then proceeds through the addition of further species to nascent crystal faces of variable surface energy. In bulk solution the structure, size, and habit of the growing crystals is regulated by a multiplicity of interrelated factors, including supersaturation, pH, temperature, and the level of additives. However, despite an extensive knowledge of these factors, the development of reliable protocols for controlling crystallization remains a challenge in solid-state chemistry.

A recent development in this area involved the use of Langmuir monolayers of surfactant molecules as molecular templates for the oriented nucleation of organic and inorganic crystals.[1-11] This

* Address correspondence to this author at the Department of Chemistry and Applied Chemistry, University of Salford, Salford M5 rWT, UK.

(1) Landau, E. M.; Grayer-Wolf, S.; Levanon, M.; Leiserowitz, L.; Lahav, M.; Sagiv, J. *Mol. Cryst. Liq. Cryst.* **1986**, *134*, 323-325.
(2) Landau, E. M.; Popovitz-Bior, R.; Levanon, M.; Leiserowitz, L.; Lahav, M.; Sagiv, J. *J. Am. Chem. Soc.* **1989**, *111*, 1436-1439.

0002-7863/92/1514-4681$03.00/0